Journal of
Marine Science and Engineering

MDPI

Article

Thermo-Economic Comparison between Three Different Electrolysis Technologies Powered by a Conventional Organic Rankine Cycle for the Green Hydrogen Production Onboard Liquefied Natural Gas Carriers

Doha Elrhoul [1,*], Manuel Naveiro [2] and Manuel Romero Gómez [2]

[1] Energy Engineering Research Group, University Institute of Maritime Studies (ETSNM), Centre for Research in Naval and Industrial Technologies (CITENI), Ferrol Industrial Campus, University of A Coruna, Paseo de Ronda 51, 15011 A Coruna, Spain
[2] Energy Engineering Research Group, University Institute of Maritime Studies (ETSNM), Nautical Sciences and Marine Engineering Department, University of A Coruna, Paseo de Ronda 51, 15011 A Coruna, Spain; manuel.naveiro@udc.es (M.N.); m.romero.gomez@udc.es (M.R.G.)
* Correspondence: doha.elrhoul@udc.es

Abstract: The high demand for natural gas (NG) worldwide has led to an increase in the size of the LNG carrier fleet. However, the heat losses from this type of ship's engines are not properly managed, nor is the excess boil-off gas (BOG) effectively utilised when generation exceeds the ship's power demand, resulting in significant energy losses dissipated into the environment. This article suggests storing the lost energy into green H_2 for subsequent use. This work compares three different electrolysis technologies: solid oxide (SOEC), proton exchange membrane (PEME), and alkaline (AE). The energy required by the electrolysis processes is supplied by both the LNG's excess BOG and engine waste heat through an organic Rankine cycle (ORC). The results show that the SOEC consumes (743.53 kW) less energy while producing more gH_2 (21.94 kg/h) compared to PEME (796.25 kW, 13.96 kg/h) and AE (797.69 kW, 10.74 kg/h). In addition, both the overall system and SOEC stack efficiencies are greater than those of PEME and AE, respectively. Although the investment cost required for AE (with and without H_2 compression consideration) is cheaper than SOEC and PEME in both scenarios, the cost of the H_2 produced by the SOEC is cheaper by more than 2 USD/kgH_2 compared to both other technologies.

Keywords: SOEC; PEME; AE; gH_2; ORC; ICE

check for updates

Citation: Elrhoul, D.; Naveiro, M.; Romero Gómez, M. Thermo-Economic Comparison between Three Different Electrolysis Technologies Powered by a Conventional Organic Rankine Cycle for the Green Hydrogen Production Onboard Liquefied Natural Gas Carriers. *J. Mar. Sci. Eng.* **2024**, *12*, 1287. https://doi.org/10.3390/jmse12081287

Academic Editors: Jian Wu, Lang Xu and Xianhua Wu

Received: 30 June 2024
Revised: 22 July 2024
Accepted: 26 July 2024
Published: 31 July 2024

1. Introduction

Liquefied natural gas (LNG) is one of the preferred options for ships in replacing conventional marine fuels, such as marine diesel oil (MDO) and heavy fuel oil (HFO), thanks to its environmentally friendly aspects [1,2]. Moreover, LNG carriers are a significant contributor to the maritime industry, transporting natural gas (NG) over the globe [3–7]. The propulsion systems of LNG carriers are classified according boil-off gas (BOG), which is mainly used for mechanical or electric propulsion [8,9], with two-stroke engines being the most popular thanks to their high efficiency compared to steam turbines and four stroke engines [10]. In order to comply with the International Maritime Organization (IMO)'s regulations and restrictions concerning the decarbonisation of the maritime sector, ship owners are required to adopt different measures related to the fuel used as well as the propulsion system, reducing the ships' emissions while improving their efficiency and flexibility [5,8,11]. The BOG generated is generally consumed by the ship's engine; however, in cases of low power demand and in order to maintain the stable pressure of the cargo tanks, excess BOG is either sent to a reliquefication plant or burned wastefully in a gas combustion unit (GCU) [1,3,8,12]. Although reliquefication plants are still adopted onboard

LNG carriers, they present disadvantages, such as their expensive cost, onboard space requirements, and the intensive energy demand [1,8,13,14].

Fernández et al. [5] suggest employing excess BOG to produce hydrogen (H_2) fuel through a steam methane reforming plant (SMR), improving the LNG carrier's efficiency, abandoning the GCU, and reducing emissions. SMR produces around three-quarters of the available H_2 thanks to both technological maturity and H_2 production costs. However, the drawbacks of this method cannot be overlooked as it relies on fossil fuel (NG), resulting in emissions, as well as onboard space limitations [1,5,15,16]. An eco-friendly alternative is to produce H_2 via electrolysis processes as oxygen (O_2) is the only by product of the water splitting reaction. Sebbahi et al. [17] presented a comparative analysis of alkaline electrolysis (AE), proton exchange membrane electrolysis (PEME), and solid oxide electrolysis (SOEC) for H_2 production using renewable sources. They concluded that although AE is the most mature electrolysis technology, it is still less efficient than PEME and SOEC, respectively. Nejadian et al. [18] conducted a comparative analysis together with techno-economic optimisation of AE, PEME, and SOEC integrated in a multi-generation energy system for power generation, water desalination, and H_2 production. They concluded that, thanks to the cooperation of both thermal and electric energy, SOEC shows a better performance in terms of H_2 production, as well as energy and exergy efficiencies, followed by PEME and AE, in this order. According to the results of the exergy–economic optimisation using Pareto frontier, the authors concluded that SOEC registers the highest system cost rate, while PEM registers the highest H_2 cost rate. Zaccara et al. [19] compared the H_2 production achieved through different renewable energy processes: PEME, SOEC, and biomass gasification, coupled with methanol and methane synthesis included in the steel industry. The results demonstrated that the H_2 produced through biomass is less pure than that produced through both PEME and SOEC, in addition to carbon dioxide (CO_2) production. SOEC consumes less water and energy compared to PEME and is more attractive if high temperatures and waste heat sources are available. Nasser and Hassan [20] compared two different systems that included SOEC and PEME powered by waste heat obtained via steam and organic Rankine cycles. They concluded that the steam Rankine cycle (SRC) shows a better performance than the organic Rankine cycle (ORC) and the SOEC is more efficient, operates more effectively, and has a lower H_2 production cost than PEME. Ferrero et al. [21] conducted a comparative analysis between high-temperature (SOEC) and low-temperature (PEME) electrolysis for H_2 production. They concluded that, at the same H_2 production rate and pressure, SOEC is more efficient and shows a better performance than PEME. Dere et al. [22] studied H_2 production onboard ships through PEME powered by the waste heat of the engine's excess exhaust gases. The results of this study show that the fuel consumption is reduced by 0.5% and achieved a USD 42,740 annual saving thanks to waste heat recovery. Wang et al. [23] conducted a comprehensive thermodynamic analysis of an SOEC powered by a marine engine's waste heat through an ORC for H_2 production and power load adjustment. The results show that the proposed system recovers 44.13% of the engine's waste heat, producing 0.431 kg/s of H_2.

According to the aforementioned literature review, there exists no article that thermo-economically compares the three electrolysis technologies for maritime transport. Hence, the novelty of this article lies in the comparison of the H_2 production onboard LNG carriers through different electrolysis processes coupled separately with an ORC system recovering the waste heat (WH) from both the ship's engine and the BOG excess. The H_2 produced is compressed for use when required.

The article is divided as follows: first, Section 2 compares the main characteristics of the three studied electrolysis processes, then Section 3 is dedicated to the overall systems description (ORC, electrolysis processes, H_2 compression plant). The electrochemical modelling of the different electrolysers' stacks is presented in Section 4, while Section 5 outlines the economic analysis of the overall systems. Finally, the simulations results are presented in Section 6 for a better understanding and comparison of the overall H_2 production systems.

2. Comparison between the Different Electrolysis Technologies

Table 1 compares the main characteristics of the low- and high-temperature electrolysis technologies studied in this article, namely AE, PEME, and SOEC electrolysis. AE is a cheap technology operating at low pressures and temperatures; however, it is hindered using corrosive liquid electrolytes, has low current densities, and has a low H_2 purity requiring an additional H_2 purification stage [24–26]. Unlike AE, PEME is characterised by high current densities and a non-corrosive solid electrolyte. The main drawback of this technology is the need for ultra-pure feed water and expensive equipment such as the membrane and noble metal electrodes [24–26]. SOEC is a high-temperature electrolysis that is still under investigation; high efficiency and low energy consumption play in favour of this technology. The high temperature and thermal cycles of SOEC are limiting, respectively, its application and the materials' lifetime [24–26].

Table 1. Comparison between the different electrolysis technologies [24–31].

		Low-Temperature Electrolysis		**High-Temperature Electrolysis**
		AE	**PEME**	**SOEC**
Semi-reactions	Anode	$2OH^- \rightarrow H_2O + \frac{1}{2}O_2 + 2e^-$	$H_2O \rightarrow 2H^+ + \frac{1}{2}O_2 + 2e^-$	$O^{2-} \rightarrow \frac{1}{2}O_2 + 2e^-$
	Cathode	$2H_2O + 2e^- \rightarrow H_2 + 2OH^-$	$4H^+ + 4e^- \rightarrow 2H_2$	$H_2O \rightarrow 2H^+ + O^{2-}$
Overall reaction		$2H_2O \rightarrow 2H_2 + O_2$	$2H_2O \rightarrow 2H_2 + O_2$	$2H_2O \rightarrow 2H_2 + O_2$
Electrolyte		Potassium hydroxide (KOH): 20–40 wt% [24,30]	Solid polymer electrolyte (Perfluoro sulfonic acid (PFSA)), usually Nafion®	Yttria stabilised zirconia (YSZ)
		Sodium hydroxide (NaOH): 20 wt% [24]		
Anode electrode		Nickel coated perforated Ni-Co alloys Stainless steel Metal oxides	Platinum carbon RuO_2, IrO_2 Graphite-PTFE + Ti/RuO_2, IrO_2	Perovskites (LSCF, LSM) Ceramics (Mn, La, Cr) YSZ
Cathode electrode		Nickel coated perforated Ni-Mo alloys Ni-Co alloys Steel + Ni	Iridium oxide Pt, Pt-Pd Graphite + Pt/Pt	Ni/YSZ Zr + Ni/CeOx
Operating temperature (°C)		20–90	20–100	600–1200
Operating pressure (bar)		1–30	<70 [25,27,29]	1 [25,27–29]
			70 [28]	<20 [26]
			<200 [26,30]	1–5 [24]
			1–350 [24]	<25 [30]
Voltage range (V)		1.4–3	1.4–2.5	0.7–1.5
Current density (A/m^2)		2000–8000	0–20,000	0–20,000
Cell area (m^2)		1–3 [25]	<0.15 [25]	0.02 [25]
		<4 [26,30]	<0.13 [26]	<0.06 [26]
			<0.3 [30]	<0.01 [30]

Table 1. *Cont.*

		Low-Temperature Electrolysis		High-Temperature Electrolysis
		AE	**PEME**	**SOEC**
Stack energy consumption (kWh/Nm^3)		4.2–5.9	4.2–5.5	>3.2
System energy consumption (kWh/Nm^3)		4.5–6.6 [26,30]	4.2–6.6 [26,30]	3.7–3.9 [26,30]
		5.55 [32]	5.4 [32]	3.8 [32]
Stack efficiency (%LHV)		50–78	50–83	80–100
System efficiency (%LHV)		51–60	46–60	76–81
Stack capital cost (USD/kW)	Minimum 1 MW	270	400	>2000
	Minimum 10 MW	500–1000	700–1400	Unknown
Maintenance cost (% of investment cost/year)		2–3 [33]	3–5 [33]	Unknown [33]
Stack lifetime (h)		60,000–120,000	20,000–100,000	8000–20,000
Maturity (Technology readiness level TRL)		Mature and commercial TRL 9	Commercial at small and medium scales TRL 8 expected to reach 9 by 2050	Development phase TRL 6 expected to reach 9 by 2050
Advantages		Cheap No need for noble metal electrocatalysts Long-term stability Reliable functioning	Space saving configuration High H_2 purity Fast start-up Non-corrosive solid electrolyte High current densities High production rate	Cheap High efficiency No need for noble metal electrocatalysts High working temperature Low pressure Low energy consumption Non-corrosive solid electrolyte Low pure water requirement
Disadvantages		Low H_2 purity Low current densities Slow start-up Corrosive High energy consumption	Expensive membrane and electrodes Acidic environment High pressure Ultra-pure feed water	Limited stability Small cell area Safety issues Limited application Under development

3. Systems Description

This section describes the possible H_2 production chain (energy recovery, H_2 production and its compression) onboard LNG carriers. As depicted in Figure 1, an organic Rankine cycle is used to recover all the available onboard waste heat and deliver it to the electrolysis stack (AE, PEME, or SOEC) for the H_2 production. The H_2 produced is then compressed to be used as a clean fuel when needed.

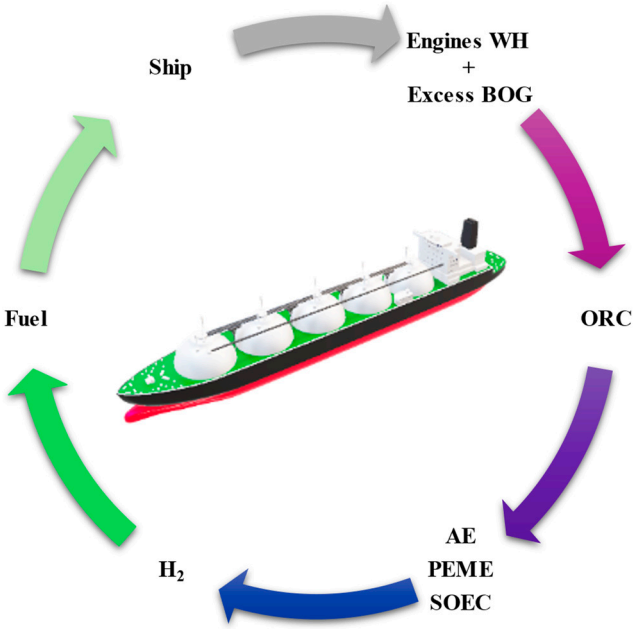

Figure 1. Overall H_2 production system. (Ship source: [34]).

3.1. Ship Model and Characteristics

The study adopts an LNG ship model propelled mechanically with two principal two-stroke engines and four auxiliary four-stroke dual fuel engines. The engines' data are extracted from MAN-CEAS [35] and the project guide [36], respectively. The engine wastes heat through different stream sources, mainly from the jacket water (JW), scavenge air (SA), and exhaust gases (EG). For simplification and consistency in calculation, the data collected from the engines are correlated with the Engineering Equation Solver (EES), generating equations for the WH streams and the specific energy consumption as a function of the ship's load (set to a value of 70% for the principal engines and 80% for the auxiliary engines). The main ship characteristics are summarized in Table 2.

Table 2. Main characteristics of the model LNG carrier.

Ship's Characteristic	Value
Total cargo capacity (V_{tank})	1.7×10^5 m^3
Propulsion system	Mechanical 2-stroke
Principal engine type	2 × MAN–5G70 ME-C10.5
Propulsion power (MCR)	2 × 12,835 kW (70.8 rpm)
Auxiliary engines type	2 × 6H35DF
	2 × 7H35DF
Auxiliary power (MCR)	2 × 2880 kW
	2 × 3360 kW
Auxiliary power demand	3448 kW
Total steam consumption	1999.2 kg/h
Boil-off rate (BOR)	0.10%
Freshwater generation ($\dot{m}_{FWG}$)	20,000 kg/day

The heat needed (Q_{FWG}) to generate a given freshwater flow rate is calculated by Equation (1) with 15% of tolerance (t_{FWG}) [37]:

$$Q_{FWG} = \frac{\dot{m}_{FWG}}{0.03(1 - t_{FWG})} \tag{1}$$

The mass flow rate ($\dot{m}_{BOG}$) of the BOG extracted from the LNG tanks is calculated by the following equations:

$$\dot{m}_{BOG} = \dot{m}_{BOG_N} - \frac{\rho_{BOG}}{\rho_{LNG}}\left(\dot{m}_{LNG} + \dot{m}_{BOG_N}\right) \tag{2}$$

$$\dot{m}_{BOG_N} = BOR \cdot V_{tank} \cdot \rho_{LNG} \tag{3}$$

where $\dot{m}_{LNG}$ and $\dot{m}_{BOG_N}$ are the mass flow rate of the LNG extracted from the tanks and the natural BOG, respectively; ρ_{BOG} and ρ_{LNG} are the BOG and LNG densities; V_{tank} is the total cargo capacity; and BOR is the boil-off rate [38].

3.2. Waste Heat Recovery System (ORC)

Recovering the waste heat onboard ships is advantageous as it improves the ships' energy efficiency and reduces the fuel consumption, which is turn results in lower emissions and reduced operating costs [39–41]. Among the different waste heat recovery (WHR) cycles, organic Rankine cycles (ORCs) are commonly studied in the literature and widely used for the WHR onboard marine vessels [39,40]. ORCs are an attractive system to recover the waste heat and convert it to a useful power [42–44]. They are characterised by their simplicity and the use of affordable and readily available components (similar to those in a refrigeration system), as well as their ability and flexibility to recover heat from both low- and medium-temperature sources, such as the scavenge air and jacket water [39,45,46]. Choosing the right ORC working fluid is tricky, as it involves considering several factors, including environmental impact, operating conditions (e.g., pressures and temperatures), and economic considerations [39]. This study adopts R245fa as the ORC's working fluid (WF). Abdul Qyyum et al. [47] assessed various WFs and concluded that, among the 95 studied, R245fa is the most commonly used and optimal WF for ORC systems. In addition, despite the high global warming potential (GWP) of R245fa that reaches a value of 1030, it is a suitable WF for the WHR from marine engines [42,48,49], and it has many advantages such as the low pump power consumption, availability, nonflammability, high net power output, fire hazard reduction, and payback minimisation [42,47,50,51]. Table 3 summarised the key parameters of R245fa.

Table 3. Main characteristics of the working fluid R245fa [47,48,50,52].

Working Fluid Characteristic	Value
ASHRAE code	R245fa
Chemical name	Pentafluoro-propane
Chemical formula	$CF_3CH_2CHF_2$
Type	Dry
ASHRAE safety group	B1
ODP	0
GWP	1030
Critical temperature (°C)	154
Critical pressure (bar)	36.5
Normal boiling point (°C)	15.14

Figure 2 illustrates the ORC configuration adopted in this article. The organic fluid R245fa is pressurised (2) by the pump (P1), then preheated and vaporised through the different WHR streams (JW, SA, and EG) of the multi-streams heat exchanger (MSHEX). The resulting saturated vapor (3) is expanded in the turbine (T), producing mechanical power that is converted to electric energy through a generator (G). Hence, supplying the ship's utility services with their power needs and providing the remaining energy to the electrolysis stacks. The remaining fluid (4) leaving the turbine is condensed back to a liquid state (1) and returned to the pump for a new cycle. The economiser (ECO) is used to preheat the steam required by the ship services, as well as for an additional water preheating process in the case of SOEC. Freshwater is secured onboard the ship through a freshwater generator (FWG) by using the available heat supplied by the JW.

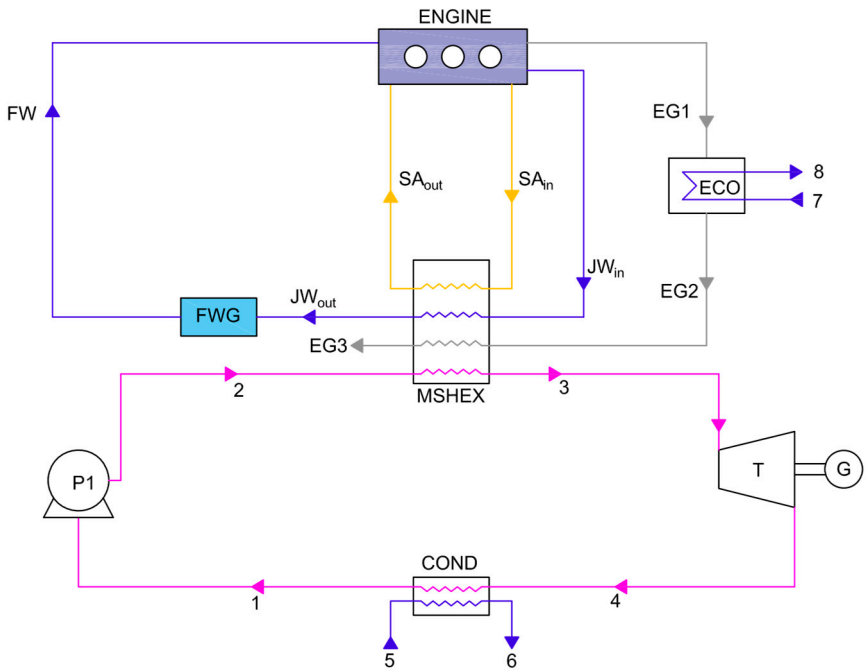

Figure 2. WHR system through an ORC.

The ORC energy efficiency (η_{ORC}) as well as the available ($\eta_{av,\ LHV}$) and recovered ($\eta_{rec,\ LHV}$) system efficiencies are determined as follows:

$$\eta_{ORC} = \frac{W_{Turb} - W_{Pump}}{Q_{WHR-in}} \tag{4}$$

$$\eta_{av,\ LHV} = \frac{\dot{m}_{H_2-prod} \cdot LHV_{H_2}}{Q_{av}} \tag{5}$$

$$\eta_{rec,\ LHV} = \frac{\dot{m}_{H_2-prod} \cdot LHV_{H_2}}{Q_{rec}} \tag{6}$$

where Q_{WHR-in} is the heat recovered from the engines WH streams, and Q_{av} refers to all the available WH, while Q_{rec} is only the WH recovered and used. W_{Turb} and W_{Pump} are the mechanical works of the ORC turbine and pump. $\dot{m}_{H_2-prod}$ is the mass flow rate of the H_2 produced, and LHV_{H_2} is its lower heating value.

3.3. Hydrogen Production Systems

Although H_2 production through electrolysis contributes only 4% of the total worldwide production [53], it is considered the cleanest process since O_2 is the only by-product of the H_2O splitting reaction. In addition, H_2 production onboard ships through electrolysis

is more advantageous than steam methane reforming (SMR) due to its ease of use and compactness. This subsection describes the different layouts of electrolysis technologies adopted in this article, namely AE, PEME, and SOEC.

3.3.1. AE Layout

The configuration of the AE adopted in this article is depicted in Figure 3. A molar fraction of 80% H_2O is mixed with 20% of an alkaline electrolyte (9), KOH in this study. The H_2O needed for the electrolysis process (10) is pumped (11) and mixed (13) with the O_2 derived from the anode electrode (12). The O_2 produced (14) and the H_2 gas leaving the cathode electrode (16) are separated from the electrolyte (22, 23) through separators (S1 and S2), respectively, at a pressure drop of 0.3 bar. The H_2 gas produced (18) is separated from the remaining H_2O (21) and undergoes further separation through (S4) to ensure its purity (19). The electrolyte residues (24) are pumped to the initial pressure (7 bar) and temperature (75 °C), then returned back to the stack (25).

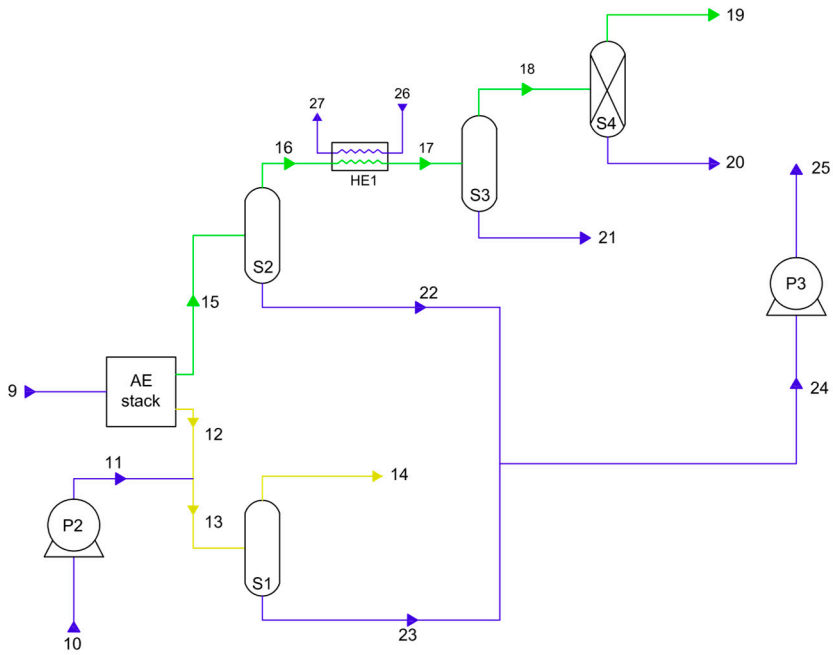

Figure 3. AE layout for onboard H_2 production.

3.3.2. PEME Layout

The PEME configuration, adopted from [19], is illustrated in Figure 4. H_2 and O_2 migrate the cathode (16) and anode (10) electrodes, respectively. Part of the H_2 produced gas (17) permeates through the membrane to the anode electrode (18), while part of the O_2 gas permeates to the cathode electrode (11). The permeation coefficient is calculated according to Equations (7) and (8). On one hand, the permeated O_2 is mixed (20) with the H_2 (19) derived from the cathode at 15 bar, cooled to 30 °C, then separated (22) from any H_2O residues (25). The H_2 gas is further purified (23) through S3. On the other hand, the permeated H_2 is mixed with O_2 (13) at 10% of the cathode pressure (1.5 bar), and the O_2 produced (15) is also separated from H_2O residues (27). The pressure of the remaining H_2O from O_2 (27) and H_2 (25) separation is reduced to atmospheric pressure, mixed with the recycled H_2O (29), and then returned back to the stack (31) at 15 bar and 30 °C.

$$H_{2perm} = \left(0.0009 \cdot e^{0.025 \cdot T}\right) \cdot \Delta P \cdot A_{cl} \tag{7}$$

$$O_{2perm} = \frac{H_{2perm}}{2} \tag{8}$$

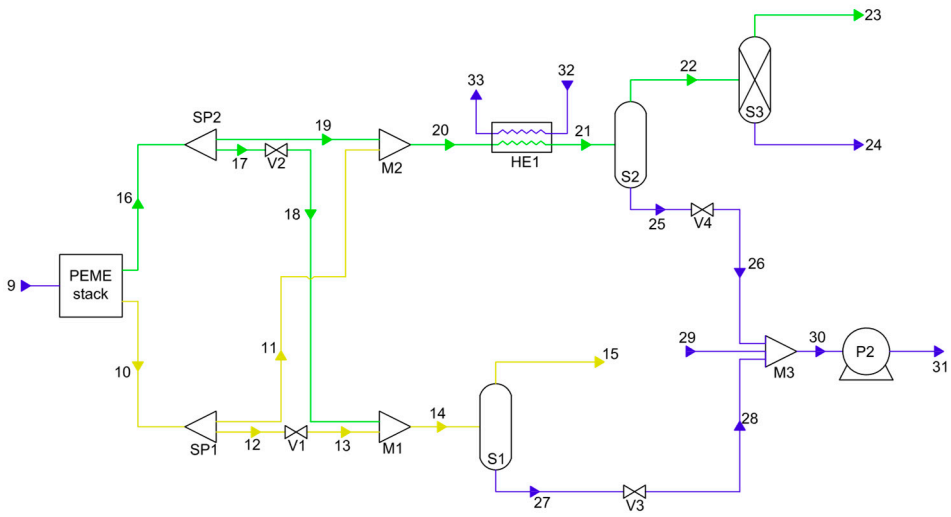

Figure 4. PEME layout for onboard H_2 production.

3.3.3. SOEC Layout

Figure 5 illustrates the SOEC configuration used in this article. A molar fraction of 90% H_2O and 10% H_2 are mixed (14) in the SOEC stack. H_2 and O_2 ions migrate to the cathode (15) and anode (10) electrodes, respectively. In order to simplify the calculations, the O_2 sweep gas flow (9) is neglected in this study. On one hand, H_2 leaves the cathode at 800 °C and then exchanges heat gradually with H_2O through a series of heat exchangers (HE1, HE2, and HE3), decreasing its temperature to 30 °C (18). The H_2 is separated (19) and purified (20) from any residues. The remaining H_2O (23, 24) and H_2 (22) are recycled to be used in the H_2 cooling process (26, 30), along with the water makeup (25). The H_2 produced (21) is compressed for subsequent use as required. On the other hand, O_2 leaving the anode at 800 °C is separated (12) from any O_2 sweep gas (11), then cooled through (HE4) and released to the environment (13). The slightly heated H_2O (27) is reheated (28) by the steam coming from the ORC (33) and used for the O_2 cooling process in HE4. The resulting steam (29) is mixed with the recycled H_2 (22), reforming the initial composition (90% H_2O + 10% H_2), while the temperature is raised to 800 °C.

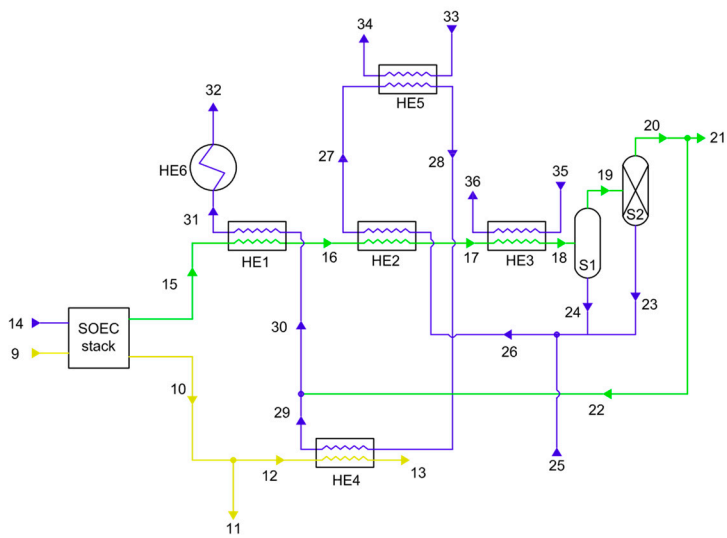

Figure 5. SOEC layout for onboard H_2 production.

3.4. Hydrogen Compression System

Among the different possible H_2 storage methods, compressed H_2 is the most commonly used due to its simplicity and technological maturity [54,55]. Figure 6 illustrates

the H_2 compression stages, the H_2 produced (37) through the different studied electrolysis processes (AE, PEME, or SOEC) is separated (38) from any possible remaining H_2O (49), then compressed through the compressors (C_i) at a constant pressure ratio, achieving a compression pressure of 150 bar. After each compression, the H_2 is cooled down to 30 °C through HE6, HE7, and HE8, then separated from H_2O residues. The compressed H_2 (47) undergoes another purification process (S9), ensuring the resulting H_2 is pure (48).

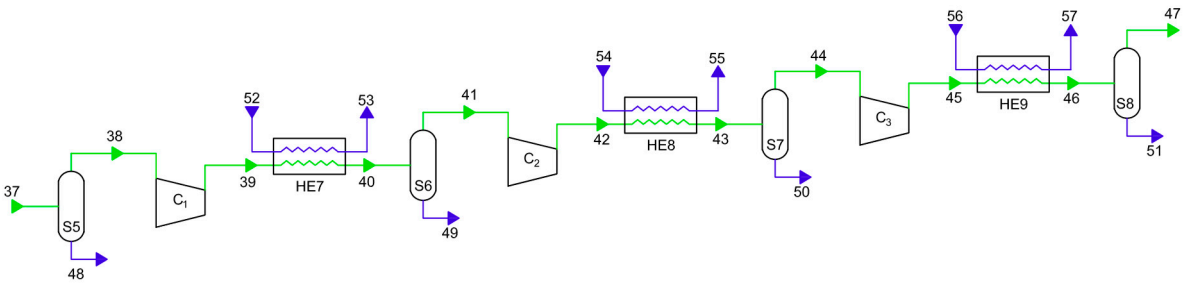

Figure 6. H_2 compression system.

4. Electrochemical Modelling of the Electrolysis Stacks

Developing an electrochemical model of the electrolysis stacks is crucial for assessing the water splitting process. The stacks are modelled using Aspen Custom Modeler V12.1 (ACM), then exported to Aspen Hysys V12.1 for simulation with the rest of the systems' components. An in-depth and comprehensive study of the electrochemical equations related to the different water electrolysis (AE, SOEC, and PEME) is already presented in the open literature. The following subsections will briefly state the necessary equations used in the electrochemical modelling according to each electrolysis stack type.

4.1. Standard Electrochemical Equations

Both heat and electricity sources are mandatory inputs to drive the splitting reactions in the different stacks [23,56]. The electric power input (W_{el}) is calculated as follows [18,57]:

$$W_{el} = V_{st} \cdot I_{st} \tag{9}$$

$$V_{st} = V_{cl} \cdot N_{cl} \tag{10}$$

$$I_{st} = J \cdot A_{cl} \tag{11}$$

where V_{st} and V_{cl} are, respectively, the stack and cell voltages, I_{st} is the stack current, J the current density, A_{cl} the cell area, and N_{cl} the stack number of cells.

The heat required/generated (Q_{st}) by the electrolysis stack is determined by Equation (12) [24,58], deciding if the electrolysis process operates in an endothermic ($Q_{st} < 0$), exothermic ($Q_{st} > 0$), or thermoneutral ($Q_{st} = 0$) mode:

$$Q_{st} = I_{st} \cdot N_{cl} \cdot (V_{cl} - V_{th}) \tag{12}$$

$$V_{th} = \frac{\Delta H}{2F} \tag{13}$$

where V_{th} is the thermoneutral voltage, ΔH is the total energy consumption, and F the Faraday constant.

The heat losses (Q_{losses}) are calculated in this study as 10% of the electrolysis thermal heat (Equation (14)), while the heat excess (Q_{excess}), if any, is determined by applying the global energy balance (Equation (15)):

$$Q_{losses} = 10\% \cdot |Q_{st}| \tag{14}$$

$$Q_{excess} = Q_{st} - Q_{losses} \tag{15}$$

The energy (η_{en-LHV}) and exergy (η_{ex}) efficiencies of the electrolysis stacks are assessed by Equations (16) and (17) as follows:

$$\eta_{en-LHV} = 100 \cdot \frac{\dot{m}_{H_2-prod} \cdot \mathrm{LHV}_{H_2}}{W_{el} + Q_{in-heat}} \tag{16}$$

$$\eta_{ex} = \frac{\dot{n}_{H_2-prod} \cdot E_{H_2}}{E_{el} + E_{heat}} \tag{17}$$

$$E_{el} = W_{el} \tag{18}$$

$$E_{heat} = Q_{in-heat}\left(1 - \frac{T_0}{T}\right) \tag{19}$$

where $Q_{in-heat}$ is the sum of all heat inputs required by the electrolysis stack, LHV_{H_2} is the H_2 lower heating value, $\dot{m}_{H_2-prod}$ and $\dot{n}_{H_2-prod}$ are the mass and molar flow rates of the H_2 produced, respectively, E_{H_2} is the H_2 standard chemical exergy, E_{el} and E_{heat} are the rate of the electric and thermal exergy inputs, T is the stack temperature, and T_0 the reference environment temperature.

4.2. AE Stack Modelling

The electrochemical modelling of the AE stack is based on the equation used by [24,59,60]. In general, the cell voltage required for an electrolysis is the sum of the reversible voltage and the voltages generated by irreversible losses. Sánchez et al. [59] have developed comprehensive equations (Equations (20) and (22)) to calculate the cell (V_{cl}) and reversible (V_{rev}) voltages using empirical correlations as functions of the stack temperature (T) and pressure (P) as follows [60]:

$$V_{cl} = V_{rev} + ((r_1 + d_1) + r_2 T + d_2 P) \cdot J + s \cdot log\left[\left(t_1 + \frac{t_2}{T} + \frac{t_3}{T^2}\right) \cdot J + 1\right] \tag{20}$$

$$V_{rev} = V_{rev}^0 + \frac{RT}{zF} ln \frac{[H_2][O_2]^{0.5}}{[H_2O]} \tag{21}$$

$$V_{rev} = a_1 - a_2 T + a_3 T ln(T) + a_4 T^2 + a_5 T ln(P) + a_6 P - a_7 \frac{P}{T} - a_8 \frac{P^2}{T} + a_9 \frac{P^2}{T^{3/2}} + a_{10} \frac{P^2}{T^2} - a_{11} \frac{P^2}{T^3} \tag{22}$$

where r_i, d_i, t_i, a_i, and s are constant parameters obtained by [24] through experiment (Table 4), and J is the current density traversing the AE stack.

Faraday efficiency ($\eta_{faraday}$) is calculated to measure the AE process effectiveness [57]. In general, $\eta_{faraday}$ is the ratio (Equation (23)) between the actual $\left(\dot{m}_{H_2-prod}\right)$ and theoretical $\left(\dot{m}_{H_2-theor}\right)$ H_2 production rate based on the consumed intensity. $\eta_{faraday}$ is also known as the "current efficiency" due the effect of the parasitic current losses throughout the gas conduits [61], these later are affected by the temperature while the pressure has a slight influence [57]; hence, for a given temperature, $\eta_{faraday}$ can be expressed by an empirical equation based on the four related parameters f_{ij} presented in Table 5 (Equation (24)) [57,59,61]:

$$\eta_{faraday} = \frac{\dot{m}_{H_2-prod}}{\dot{m}_{H_2-theor}} \tag{23}$$

$$\eta_{faraday} = 100 \cdot \left(\frac{J^2}{f_{11} + f_{12} T + J^2}\right) \cdot (f_{21} + f_{22} T) \tag{24}$$

Table 4. Experimental parameters used for the calculation of the AE cell voltage [24,57,59].

Parameter	Value	Unit
	Cell voltage	
r_1	4.45153×10^{-5}	$\Omega\ m^2$
r_2	6.88874×10^{-9}	$\Omega\ m^2/°C$
t_1	−0.01539	m^2/A
t_2	2.00181	$m^2\ °C/A$
t_3	15.24178	$m^2\ °C^2/A$
d_1	-3.12996×10^{-6}	$\Omega\ m^2$
d_2	4.47137×10^{-7}	$\Omega\ m^2/bar$
s	0.33824	V
	Reversible voltage	
a_1	1.5184	V
a_2	0.0015421	V/K
a_3	0.00009523	V
a_4	0.0000000984	V/K^2
a_5	0.000064629	V/K bar
a_6	0.000021946	V/bar
a_7	0.0055433	V·K/bar
a_8	0.0000095196	$V{\cdot}K/bar^2$
a_9	0.00013914	$V{\cdot}K^{3/2}/bar^2$
a_{10}	0.0026144	$V{\cdot}K^2/bar^2$
a_{11}	0.4953	$V{\cdot}K^3/bar^2$

The molar flow rates of the H_2O consumed ($\dot{n}_{H_2O-cons}$) during the AE process as well as the H_2 ($\dot{n}_{H_2-prod}$) and O_2 ($\dot{n}_{O_2-prod}$) produced are calculated by the following equations:

$$\dot{n}_{H_2-prod} = \eta_{faraday} \cdot \frac{J \cdot A_{cl} \cdot N_{cl}}{2F} \tag{25}$$

$$\dot{n}_{H_2O-cons} = \dot{n}_{H_2-prod} \tag{26}$$

$$\dot{n}_{O_2-prod} = \frac{\dot{n}_{H_2-prod}}{2} \tag{27}$$

According to [24,57], during the AE process, part of the H_2 flow ($\dot{n}_{HTO}$) is diffused into the O_2 channel (from cathode to anode) through AE diaphragms. The amount of $\dot{n}_{HTO}$ is expressed by Equation (28) using the hydrogen to oxygen (HTO) diffusion coefficient Equation (29). The counter-diffusion (oxygen to hydrogen (OTH)) is neglected due to the small amount (0.1 to 0.5%) of the O_2 is diffused to the H_2 channel [57]:

$$\dot{n}_{HTO} = \frac{HTO \cdot \dot{n}_{O_2-prod}}{1 - HTO} \tag{28}$$

$$\begin{aligned} HTO = \left(C_1 + C_2T + C_3T^2\right) + \left(C_4 + C_5T + C_6T^2\right) exp\left(\frac{C_7 + C_8T + C_9T^2}{J}\right) + \left(E_1 + E_2P + E_3P^2\right) \\ + \left(E_4 + E_5P + E_6P^2\right) exp\left(\frac{E_7 + E_8P + E_9P^2}{J}\right) \end{aligned} \tag{29}$$

where C_i and E_i are the gas purity parameters related to the temperature (T) and pressure (P), respectively, their values are summarised in Table 5.

Table 5. Faraday and HTO diffusion experimental parameters used for AE stack modelling [24,57,59].

Parameter	Value	Unit
	Faraday efficiency	
f_{11}	478,645.74	A^2/m^4
f_{12}	−2953.15	A^2/m^4 °C
f_{21}	1.03960	--
f_{22}	−0.00104	$°C^{-1}$
	Hydrogen to oxygen diffusion	
C_1	0.09901	--
C_2	−0.00207	$°C^{-1}$
C_3	1.31064×10^{-5}	$°C^{-2}$
C_4	−0.08483	--
C_5	0.00179	$°C^{-1}$
C_6	-1.13390×10^{-5}	$°C^{-2}$
C_7	1481.45	A/m^2
C_8	−23.60345	A/m^2 $°C^1$
C_9	−0.25774	A/m^2 $°C^2$
E_1	3.71417	--
E_2	−0.93063	Bar^{-1}
E_3	0.05817	Bar^{-2}
E_4	−3.72068	--
E_5	0.93219	Bar^{-1}
E_6	−0.05826	Bar^{-2}
E_7	−18.38215	A/m^2
E_8	5.87316	A/m^2 Bar
E_9	−0.46425	A/m^2 Bar^2

The AE electrodes are submerged in a KOH electrolyte. Hence, the molar flow rates of H_2, O_2, H_2O, and KOH at the anode and cathode are calculated as follows:

Anode:

$$\dot{n}_{H_2-an} = \dot{n}_{HTO} \tag{30}$$

$$\dot{n}_{O_2-an} = \dot{n}_{O_2-prod} \tag{31}$$

$$\dot{n}_{H_2O-an} = \frac{\dot{n}_{H_2O-in} - \dot{n}_{H_2O-cons}}{2} \tag{32}$$

$$\dot{n}_{KOH-an} = \frac{\dot{n}_{KOH-in}}{2} \tag{33}$$

Cathode:

$$\dot{n}_{H_2-cat} = \dot{n}_{H_2-prod} \tag{34}$$

$$\dot{n}_{O_2-cat} = 0 \tag{35}$$

$$\dot{n}_{H_2O-cat} = \dot{n}_{H_2O-an} \tag{36}$$

$$\dot{n}_{KOH-cat} = \dot{n}_{KOH-an} \tag{37}$$

$\dot{n}_{KOH-in}$ and $\dot{n}_{H_2O-in}$ are known molar inlet flows of KOH and H_2O.

AE Stack Validation

In order to validate the AE stack modelling, the cell voltage–current density curve is compared with the curve obtained by Sánchez et al. [57] and the Aspentech modified modelling version [60] under the conditions presented in Table 6. According to Figure 7, the curve displays a significant concordance with the existing findings.

Table 6. Input data for the AE simulation and validation [57,60].

Variable	Value	Unit
T	75	°C
P	7	Bar
W_{el}	10	kW
N_{cl}	12	--
A_{cl}	0.1	m^2
$\dot{m}_{in}$	900	Kg/h
Inlet composition (H_2O–KOH)	35–65	% Mass fraction basis

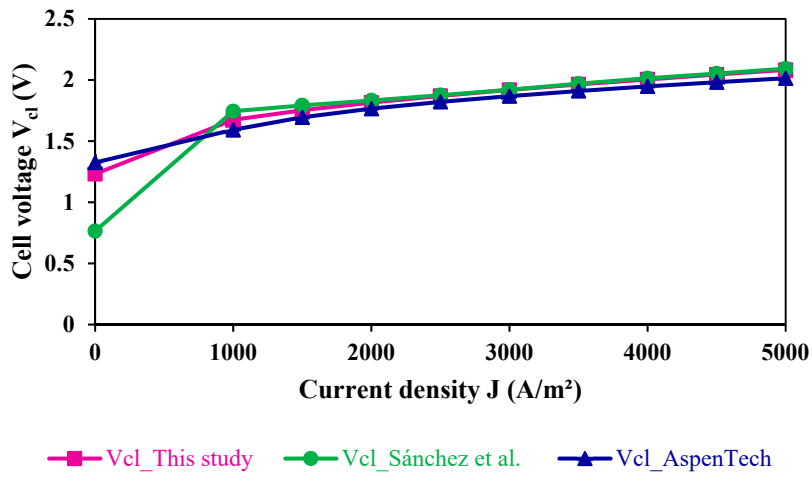

Figure 7. Validation curve of AE cell voltage–current density with [57,60].

4.3. PEME Stack Modelling

The PEME stack is modelled according to the equations used in research studies such as [62–64]. The cell voltage (V_{cl}) is the sum of the reversible voltage (V_{rev}) calculated by the Nernst equation, activation overpotentials (V_{act}) at both anode and cathode electrodes, and the ohmic overpotential of the electrolyte (V_{ohm}). The concentration overpotentials (V_{conc}) are negligible for high current densities not exceeding 10,000 A/m^2 [64].

$$V_{cl} = V_{rev} + V_{act} + V_{ohm} \tag{38}$$

$$V_{rev} = 1.229 - 8.5 \times 10^{-4}(T - 298) \tag{39}$$

$$V_{act} = V_{act,a} + V_{act,c} \tag{40}$$

$$V_{act,i} = \frac{RT}{F} ln\left[\frac{J}{2J_{0,i}} + \sqrt{\left(\frac{J}{2J_{0,i}}\right)^2 + 1}\right], \ (i = a, c) \tag{41}$$

$$J_{0,i} = J_{exp,i} exp\left(\frac{-E_{act,i}}{RT}\right) \tag{42}$$

$$V_{ohm} = JR_{el} \tag{43}$$

$$R_{el} = \int_0^L \frac{dx}{\sigma[\lambda(x)]} \tag{44}$$

$$\sigma[\lambda(x)] = [0.5139\lambda(x) - 0.326] \cdot exp\left[1268\left(\frac{1}{303} - \frac{1}{T}\right)\right] \tag{45}$$

$$\lambda(x) = \frac{\lambda_a - \lambda_c}{L} x + \lambda_c \tag{46}$$

where $T(K)$ is the stack temperature, $J_{0,i}$ is the exchange current density of anode (a) and cathode (c), $J_{exp,i}$ is the pre-exponential factor, $E_{act,i}$ is the activation energy, R_{el} is the overall ohmic resistance, L is the membrane thickness, $\sigma[\lambda(x)]$ refers to the local ionic conductivity of the PEME, $\lambda(x)$ is the water content at a location x in the membrane, and λ_a and λ_c are the water contents at anode and cathode membrane interfaces, while x is the distance calculated from the cathode–membrane interface. The parameters used in this study are summarised in Table 7.

Table 7. Parameters adopted for the PEME stack electrochemical modelling [63].

Parameter	Value	Unit
$J_{0,a}$	1×10^{-5}	A/m^2
$J_{0,c}$	10	A/m^2
$E_{act,a}$	76×10^3	J/mol
$E_{act,c}$	18×10^3	J/mol
L	50×10^{-6}	m
λ_a	14	--
λ_c	10	--

The molar flow rates of the H_2O reacted in the electrolysis process ($\dot{n}_{H_2O-react}$), the H_2 produced ($\dot{n}_{H_2-prod}$), and the remaining H_2O ($\dot{n}_{H_2O-out}$) are calculated by the following equations:

$$\dot{n}_{H_2O-react} = \frac{I \cdot N_{cl}}{2F} \tag{47}$$

$$\dot{n}_{H_2-prod} = \dot{n}_{H_2O-react} \tag{48}$$

$$\dot{n}_{H_2O-out} = \dot{n}_{H_2O-in} - \dot{n}_{H_2O-react} \tag{49}$$

The molar flow rates of H_2, O_2 and H_2O at cathode and anode are calculated as stated below:

Anode:

$$\dot{n}_{H_2-an} = 0 \tag{50}$$

$$\dot{n}_{O_2-an} = \frac{\dot{n}_{H_2-prod}}{2} \tag{51}$$

$$\dot{n}_{H_2O-an} = \dot{n}_{H_2O-in} - \dot{n}_{H_2O-react} \tag{52}$$

Cathode:

$$\dot{n}_{H_2-cat} = \dot{n}_{H_2-prod} \tag{53}$$

$$\dot{n}_{O_2-cat} = 0 \tag{54}$$

$$\dot{n}_{H_2O-an} = 0 \tag{55}$$

PEME Stack Validation

The cell voltage–current density curve of the PEME stack modelling is validated with the finding reported by Mohtaram et al. [65] using the data of Zaccara et al. [19] as outlined in Table 8. The curve results shown in Figure 8 are in good agreement with the findings of [65].

Table 8. Input data for the PEME simulation [19].

Variable	Value	Unit
T	90	°C
P	Cathode 15-Anode 1.5 (10%)	Bar
$\dot{n}_{H_2O-in}$	352,080	kg/h
A_{cl}	1 (*)	m^2
N_{cl}	12 (*)	--
W_{el}	1,988,900	kW

(*) Values estimated for modelling purpose.

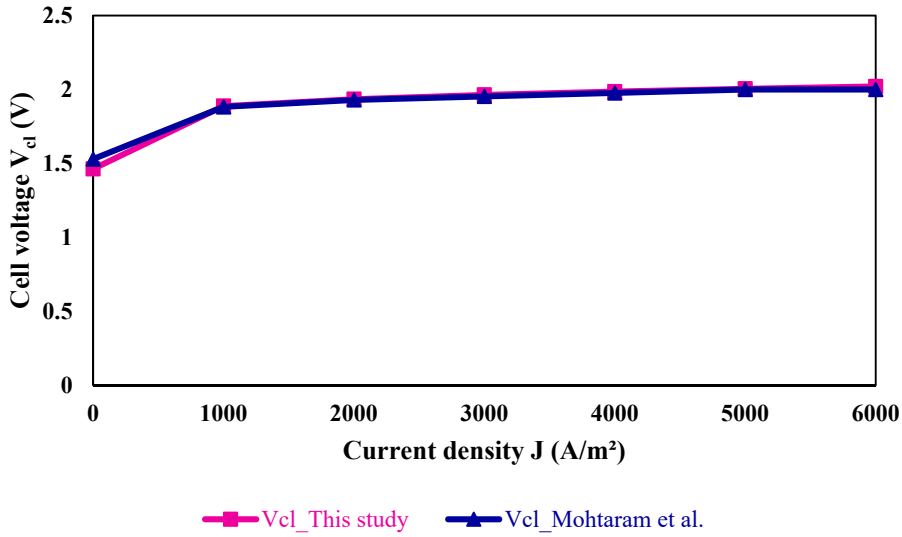

Figure 8. Validation curve of PEME cell voltage–current density with [65].

4.4. SOEC Stack Modelling

The required equations for the SOEC electrochemical modelling are extracted from research studies such as [18,23,56,66–72]. The cell voltage (V_{cl}) of the SOEC stack is calculated as the sum of the reversible voltage (V_{rev}), ohmic overpotential (V_{ohm}), activation overpotentials (V_{act}), and concentration overpotentials (V_{conc}) presented below:

$$V_{cl} = V_{rev} + V_{ohm} + V_{act} + V_{conc} \tag{56}$$

$$V_{rev} = V_0 + \frac{RT}{2F} \cdot \ln\left(\frac{P^0_{H2} \cdot \left(P^0_{O2}\right)^{1/2}}{P^0_{H2O}}\right) \tag{57}$$

$$V_0 = 1.253 - 2.4516 \cdot 10^{-4} T \tag{58}$$

$$P^0_{H_2} = y_{H_2} \cdot P \tag{59}$$

$$P^0_{O_2} = y_{O_2} \cdot P \tag{60}$$

$$P^0_{H_2O} = y_{H_2O} \cdot P \tag{61}$$

$$V_{ohm} = 2.99 \cdot 10^{-5} \cdot exp\left(\frac{10300}{T}\right) \cdot J \cdot L \tag{62}$$

where $P^0_{H_2O}$, $P^0_{H_2}$, and $P^0_{O_2}$ are the partial pressures of H_2O, H_2, and O_2, respectively, while y_{H_2O}, y_{H_2}, and y_{O_2} are the corresponding input molar fractions, V_0 the standard potential, L the electrolyte layer thickness (Table 9), J the current density, and $T(K)$ the stack temperature.

Table 9. Parameters adopted for the SOEC stack electrochemical modelling [23,73].

Parameter	Value	Unit
L	12.5×10^{-6}	m
da	17.5×10^{-6}	m
dc	12.5×10^{-6}	m
ε	0.48	--
ξ	5.4	--
rad	1.385×10^{-6}	m
ε_{H2O}/k	809.1	K
ε_{H2}/k	59.7	K
σ_{H2O}	2.641	m
σ_{H2}	2.827	m
$J_{exp,a}$	2.051×10^9	A/m^2
$J_{exp,c}$	1.344×10^{10}	A/m^2
$E_{act,a}$	1.2×10^5	J/mol
$E_{act,c}$	1×10^5	J/mol

V_{act} is calculated in the same way as in the case of PEME with the parameters summarised in Table 9. (Check Equations (40)–(42))

$$V_{conc} = V_{conc,a} + V_{conc,c} \tag{63}$$

$$V_{conc,a} = \frac{RT}{4F} \cdot ln\left(\frac{\sqrt{\left(P^0_{O_2}\right)^2 + \frac{R \cdot T \cdot J \cdot \cdot d_a}{2F \cdot B_g}}}{P^0_{O2}}\right) \tag{64}$$

$$V_{conc,c} = \frac{RT}{2F} \cdot ln\left(\frac{1 + \frac{J \cdot R \cdot T \cdot d_c}{2F \cdot D^{eff}_{H_2O} \cdot P^0_{H_2}}}{1 - \frac{J \cdot R \cdot T \cdot d_c}{2F \cdot D^{eff}_{H_2O} \cdot P^0_{H_2O}}}\right) \tag{65}$$

where d_a and d_c are the anode and cathode thickness, respectively, μ is the dynamic viscosity (Equation (66)), B_g is the flow permeability (Equation (67)), and $D^{eff}_{H_2O}$ is the effective diffusion coefficient (Equation (68)). Note that $P^0_{H_2O}$, $P^0_{H_2}$, and $P^0_{O_2}$ are in Pascal.

$$\mu = -1.692 + 889.75\left(\frac{T}{1000}\right) - 892.79\left(\frac{T}{1000}\right)^2 + 905.98\left(\frac{T}{1000}\right)^3 - 598.36\left(\frac{T}{1000}\right)^4 + 221.64\left(\frac{T}{1000}\right)^5 - 34.75\left(\frac{T}{1000}\right)^6 \tag{66}$$

$$B_g = \frac{\varepsilon^3}{72\xi(1-\varepsilon)^2}(2rad)^2 \tag{67}$$

$$\frac{1}{D^{eff}_{H_2O}} = \frac{\xi}{\varepsilon} \cdot \left(\frac{1}{D_{H_2-H_2O}} + \frac{1}{D_{H_2O-K}}\right) \tag{68}$$

where *rad* is the average pore radius, while ε and ξ are the electrode porosity and tortuosity, respectively, and their values are presented in Table 9. The Knudsen (D_{H_2O-K}) and the molecular ($D_{H_2-H_2O}$) diffusions are calculated as follows:

$$D_{H_2O-K} = \frac{2}{3} rad \sqrt{\frac{8R \cdot T}{\pi \cdot M_{H_2O}}} \tag{69}$$

$$D_{H_2-H_2O} = 0.00133 \left(\frac{1}{M_{H_2}} + \frac{1}{M_{H_2O}} \right)^{\frac{1}{2}} \frac{T^{\frac{3}{2}}}{P \cdot \left(\sigma_{H_2-H_2O}\right)^2 \cdot \Omega_D} \tag{70}$$

$$\Omega_D = \frac{1.06036}{T^{*0.1561}} + \frac{0.193}{\exp(0.47635T^*)} + \frac{1.03587}{\exp(1.52996T^*)} + \frac{1.76474}{\exp(3.89411T^*)} \tag{71}$$

$$T^* = \frac{T}{\frac{\varepsilon_{H_2-H_2O}}{k}} \tag{72}$$

$$\frac{\varepsilon_{H_2-H_2O}}{k} = \sqrt{\frac{\varepsilon_{H_2}}{k} \frac{\varepsilon_{H_2O}}{k}} \tag{73}$$

$$\sigma_{H_2-H_2O} = \frac{\sigma_{H_2} + \sigma_{H_2O}}{2} \tag{74}$$

M_j is the molecular mass of species j (j = H_2, O_2, H_2O), Ω_D is the dimensionless diffusion collision integral, and σ_{H2O} and σ_{H2} the collision diameters of steam and H_2, while ε_{H2O}/k and ε_{H2}/k are the Lennard-Jones potentials. T^* is the dimensionless temperature.

The molar flow rates of the H_2O reacted during the electrolysis process and the H_2 and O_2 produced are calculated by the following equations:

$$\dot{n}_{H_2O-react} = \frac{I \cdot N_{cl}}{2F} \tag{75}$$

$$\dot{n}_{H_2-prod} = \dot{n}_{H_2O-react} \tag{76}$$

$$\dot{n}_{O_2-prod} = \frac{\dot{n}_{H_2-prod}}{2} \tag{77}$$

On the other hand, the molar flow rates of H_2, O_2, and H_2O at the anode and cathode electrodes are determined as follows:

Anode:

$$\dot{n}_{H_2-an} = 0 \tag{78}$$

$$\dot{n}_{O_2-an} = \dot{n}_{O_2-prod} \tag{79}$$

$$\dot{n}_{H_2O-an} = 0 \tag{80}$$

Cathode:

$$\dot{n}_{H_2-cat} = \dot{n}_{H_2-prod} \tag{81}$$

$$\dot{n}_{O_2-cat} = 0 \tag{82}$$

$$\dot{n}_{H_2O-an} = \dot{n}_{H_2O-in} - \dot{n}_{H_2O-react} \tag{83}$$

SOEC Stack Validation

The cell voltage–current density curve of the SOEC stack modelling is validated with the findings of [66] using the input data of [23] (Table 10). The cell voltage–current density curve depicted in Figure 9 shows a good agreement with the findings of [66].

Table 10. Input data for the SOEC simulation [23].

Variable	Value	Unit
T	850	°C
P	1.01325	bar
$\dot{m}_{in}$	36,000	kg/h
J	8000	A/m^2
A_{cl}	0.04	m^2
N_{cl}	130,000	--
Inlet composition (H_2O–H_2)	80–20	% Molar fraction basis

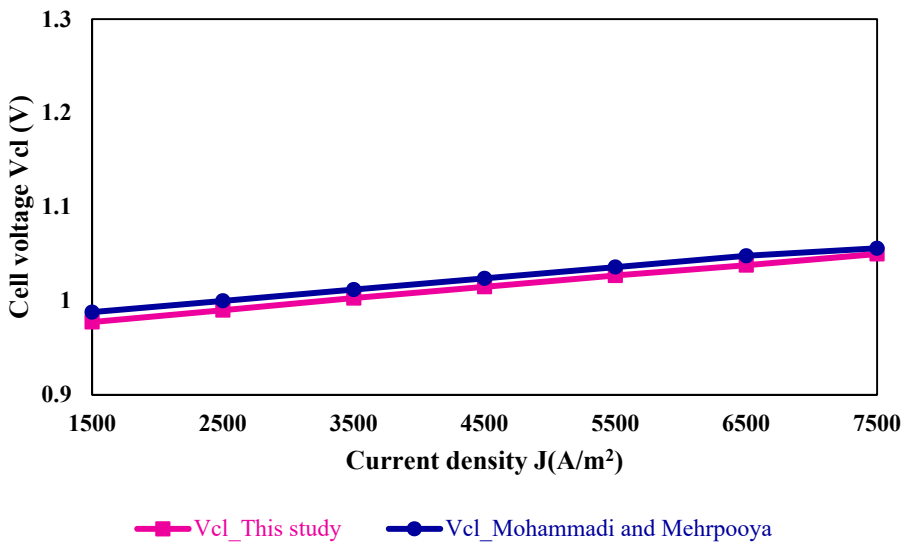

Figure 9. Validation curve of SOEC cell voltage–current density with [66].

5. Economic Analysis

The equipment cost of the three H_2 production overall systems is determined by the Aspen Process Economic Analyzer V12.1 (APEA). However, the electrolysers' cost functions are calculated separately by using the following equations [18,74]:

$$Z_{SOEC} = 2285\ (\text{USD/kW}) \cdot W_{el.SOEC} \tag{84}$$

$$Z_{PEME} = 2068\ (\text{USD/kW}) \cdot W_{el.PEME} \tag{85}$$

$$Z_{AE} = 1268\ (\text{USD/kW}) \cdot W_{el.AE} \tag{86}$$

Note that the electrolysers' cost functions are calculated for the year 2020, while the equipment cost is given for the year 2019. For accurate and significant results, the total equipment costs as well as the electrolysers' cost are updated to the same year (2022 in this study), using the chemical plant cost index (CEPCI) as shown in the following equation:

$$Z_{2022} = \frac{CEPCI_{2022}}{CEPCI_{equipment\ year}} \cdot Z_{equipment\ year} \tag{87}$$

The cost of the H_2 produced by each overall system is determined through the calculation of the levelised cost of H_2 (*LCOH*) as follows [66]:

$$LCOH = \frac{\dot{Z}_{capital\ cost} + \dot{Z}_{O\&M} + \dot{Z}_{electricity} + \dot{Z}_{fuel}}{\dot{m}_{H_2\,pr}} \tag{88}$$

$$\dot{Z}_{capital\ cost} = \frac{Z_{total} \cdot CRF}{T_{W.hr}} \tag{89}$$

$$CRF = \frac{i \cdot (1+i)^N}{(1+i)^N - 1} \tag{90}$$

$$\dot{Z}_{O\&M} = \alpha \cdot Z_{total} \tag{91}$$

where $\dot{Z}_{capital\ cost}$ is the investment cost rate, $\dot{Z}_{O\&M}$ is the operating and maintenance annual cost, and $\dot{Z}_{electricity}$ and $\dot{Z}_{fuel}$ are the electricity and fuel costs which are excluded from consideration in this study since all the energy used is that recovered from the WH without any additional energy. Z_{total} is the total equipment cost, CRF refers to the capital recovery factor, and $T_{W.hr}$ is the uptime per year, while i, N, and α are the interest rate, the plant lifetime, and the operating and maintenance factor, respectively. The parameters adopted in this study are summarised in the following Table 11:

Table 11. Parameters adopted for the economic analysis [75–77].

Parameter	Value
$T_{W.hr}$	8000 h
i	10%
N	20 years
α	3%
$CEPCI_{2019}$	607.5
$CEPCI_{2020}$	596.2
$CEPCI_{2022}$	816

6. Results and Discussion

This section is dedicated to compare the three studied electrolysis in this article (AE, PEME, and SOEC). First, the electrolysis stacks are compared, separately, between each other in Section 6.1, then an overall comparison of the onboard H_2 production system is discussed in Section 6.2. Finally, Section 6.3 presents an economic analysis of the overall systems.

6.1. Electrolysis Stacks' Comparison

The AE, PEME, and SOEC stacks are compared in this subsection using the same possible input data. The results summarised in Table 12 as well as in Figures 10 and 11 demonstrate the following:

- SOEC (3.761 kg/h) and PEME (3.760 kg/h) stacks produce more H_2 than the AE (3.652 kg/h) stack for the same current density J;
- There is a slight difference between PEME and SOEC H_2 production; however, PEME as well as AE consume more than double the energy (Wel) of SOEC;
- The cell voltage required for the SOEC process is lower than for PEME and AE,
- SOEC stack is more efficient than PEME and AE, respectively.

Table 12. Results comparison between the AE, PEME, and SOEC stacks.

Variable	Unit	AE	PEME	SOEC
T	°C	80	80	800
P	bar	1.01325	1.01325	1.01325
$\dot{m}_{in}$	kg/h	36,000	36,000	36,000
Inlet composition (molar fraction basis)	%	90% H_2O + 10% KOH	100% H_2O	90% H_2O + 10% H_2
J	A/m^2	5000	5000	5000
A_{cl}	m^2	0.04	0.04	0.04
N_{cl}	--	500	500	500
$\dot{m}_{H2\text{-}prod}$	kg/h	3.562	3.760	3.761
$\dot{m}_{O2\text{-}prod}$	kg/h	28.273	29.844	29.848
W_{el}	kW	199.97	200.46	98.93
V_{cl}	V	2.000	2.005	0.989
$\eta_{EN\text{-}LHV}$	%	59.38	62.52	97.44
η_{EX}	%	58.54	61.64	96.76

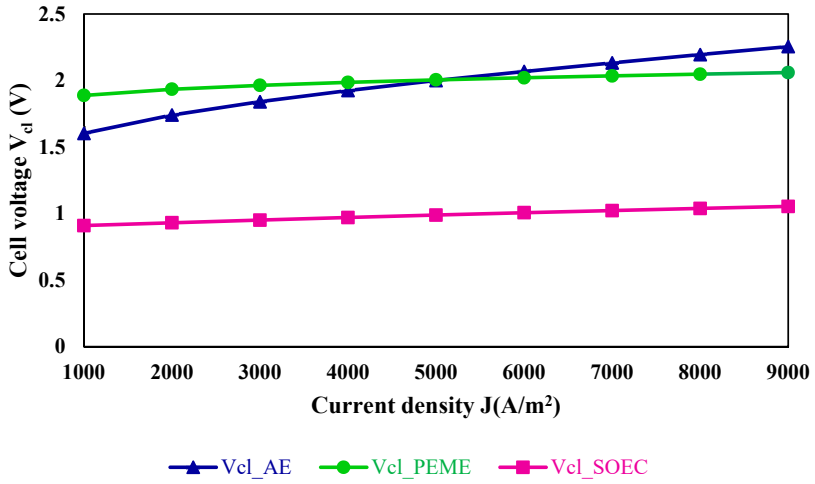

Figure 10. Cell voltage comparison between the AE, PEME, and SOEC stacks.

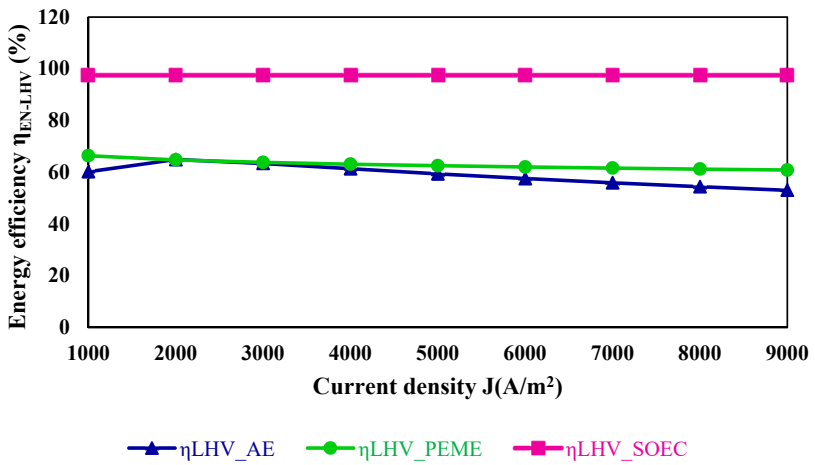

Figure 11. Energy efficiency (LHV) comparison between AE, PEME, and SOEC.

6.2. Overall Systems' Comparison

After comparing the different electrolysis stacks separately, this section compares the overall H_2 production systems from energy harvesting to the H_2 compression stage. The thermodynamic properties of the different systems are presented in the Supplementary Materials, while Table 13 outlines the input parameters of the WHR sources as a function of the engine's load which is set at a fixed value of 70%.

Table 13. WHR parameters at 70% of the engine's load.

Variable	Unit	JW	SA	EG
Temperature	°C	90.0	153.3	196.1
Pressure	bar	1.01325	1.01325	1.01325
Mass flow	kg/h	144,842	140,422	142,579
Heat flow	kW	1856	4780	3237

The input data together with the simulation results of the different H_2 production chain systems are summarised in Table 14. The results demonstrate that SOEC consumes less energy (743.53 kW) than both PEME (797.69 kW) and AE (796.25 kW) while producing more H_2 (21.94 kg/h) compared to 13.96 kg/h by PEME and 10.74 kg/h by AE. The difference in the power output between the ORC coupled with SOEC and the ORC coupled with PEME or AE is attributed to the slightly elevated temperature of the EG. This increase in temperature results from the additional heating process of the water needed by SOEC to reach the high operating temperature (800 °C).

Table 14. Comparison results of the overall H_2 production system.

Variable	Unit	AE	PEME	SOEC
Temperature	°C	80	80	800
Pressure	bar	7	15	1.01325
Inlet composition (molar fraction basis)	%	90% H_2O + 10% KOH	100% H_2O	90% H_2O + 10% H_2
A_{cl}	m^2	0.04	0.04	0.04
N_{cl}	--	500	500	500
P_{ORC}	kW	921.4	921.4	940
Q_{av}	kW	9873	9873	9873
Q_{rec}	kW	6882	6882	6910
W_{el}	kW	796.25	797.69	743.53
J	A/m^2	14,942	18,557.7	29,174.9
V_{cl}	V	2.664	2.149	1.274
$\dot{m}_{in}$	kg/h	143.5	138.6	248.2
$\dot{n}_{H_2-prod}$	kg/h	10.74	13.96	21.94
$\dot{n}_{O_2-prod}$	kg/h	85.22	110.78	174.161
η_{en-LHV}	%	44.95	58.33	64.34
η_{ORC}-av	%	8.80	8.80	8.96
η_{ORC}-rec	%	12.62	12.62	12.80
$\eta_{av,\ LHV}$	%	3.63	4.71	7.41
$\eta_{rec,\ LHV}$	%	5.20	6.76	10.59

Considering only the recovered WH, the overall system efficiency employing SOEC electrolysis is 10.59% with a stack efficiency of 64.34%$_{LHV}$ and an ORC efficiency of 12.80%, exceeding those of PEME and AE. The PEME and AE overall system efficiencies are 6.76% and 5.20%, respectively, while the stacks' efficiencies register 58.33%$_{LHV}$ and 44.95%$_{LHV}$. The ORC efficiency is 12.62% for both PEME and AE. Whether considering all the available onboard WH or solely the recovered one, the SOEC system outperforms both PEME and AE in terms of energy efficiencies, particularly the overall system efficiency, which is almost double, as well as H_2 production thanks to the high operating temperatures.

6.3. Economic Analysis of the Overall H_2 Production Systems

This subsection economically compares the overall systems using SOEC, PEME, or AE as the H_2 production process in order to decide the most viable technology to be adopted onboard maritime vessels. Tables 15–17 summarise the equipment' cost functions of the three studied systems: SOEC, PEME, and AE, respectively, considering two different scenarios: (with (SC-1) or without (SC-2) a H_2 compression plant. As mentioned before, the cost function of the electrolysers is calculated separately, the results are shown in Table 18.

Both the total equipment cost and the electrolysers' costs are updated to the same year (2022 in this study) by using the aforementioned Equation (87) for an accurate and precise comparison. As illustrated in Figure 12, excluding the H_2 compression plant (SC-2) reduces the total investment cost by more than half for all of the three overall systems studied. Including the H_2 compression system (SC-1) makes SOEC increase the plant investment cost by half a million compared to the PEME system, while excluding the compression plant plays in favour of SOEC by reducing its cost by almost USD 36,000. This is mainly due to the compressors' costs affected by the H_2 produced and the slight difference between the SOEC and PEME electrolyser's costs. AE is the cheapest system.

Table 15. Equipment costs of SOEC with and without compression plant (2022).

Equipment		SC-1	SC-2
Compressors	C1	1,329,000	
	C2	1,375,100	
	C3	1,434,500	
Condenser	COND	538,100	538,100
SOEC heat exchangers	HE1	51,900	51,900
	HE2	7800	7800
	HE3	15,400	15,400
	HE4	18,900	18,900
	HE5	11,000	11,000
	HE6	17,300	17,300
H_2 compression coolers	HE7	20,700	
	HE8	17,200	
	HE9	18,300	
Multi-streams heat exchanger	MSHEX	381,900	381,900
ORC pump	P1	33,800	33,800
ORC turbine	T	487,700	487,700
Z_{total} (USD)		5,758,600	1,563,800

Table 16. Equipment costs of PEME with and without a compression plant (2022).

Equipment		SC-1	SC-2
Compressors	C1	1,232,100	
	C2	1,266,300	
	C3	1,289,700	
Condenser	COND	546,900	546,900
PEME heat exchanger	HE1	14,300	14,300
H_2 compression coolers	HE7	14,300	
	HE8	15,000	
	HE9	16,100	
Multi-streams heat exchanger	MSHEX	548,600	548,600
ORC pump	P1	33,800	33,800
PEME pump	P2	17,000	17,000
Turbine	T	479,900	479,900
Z_{total} (USD)		5,474,000	1,640,500

Table 17. Equipment costs of AE with and without a compression plant (2022).

Equipment		SC-1	SC-2
Compressors	C1	1,232,300	
	C2	1,258,700	
	C3	1,289,700	
Condenser	COND	546,900	546,900
AE heat exchanger	HE1	13,300	13,300
H_2 compression coolers	HE7	15,000	
	HE8	14,700	
	HE9	15,200	
Multi-streams heat exchanger	MSHEX	548,600	548,600
ORC pump	P1	33,800	33,800
AE pump	P3	4400	4400
	P4	4900	4900
Turbine	T	479,900	479,900
Z_{total} (USD)		5,457,400	1,631,800

Table 18. Electrolysers' cost (2020).

Electrolyser Type	Power (kW)	Cost (USD)
SOEC	743.53	1,698,975
PEME	797.69	1,649,620
AE	796.25	100,964

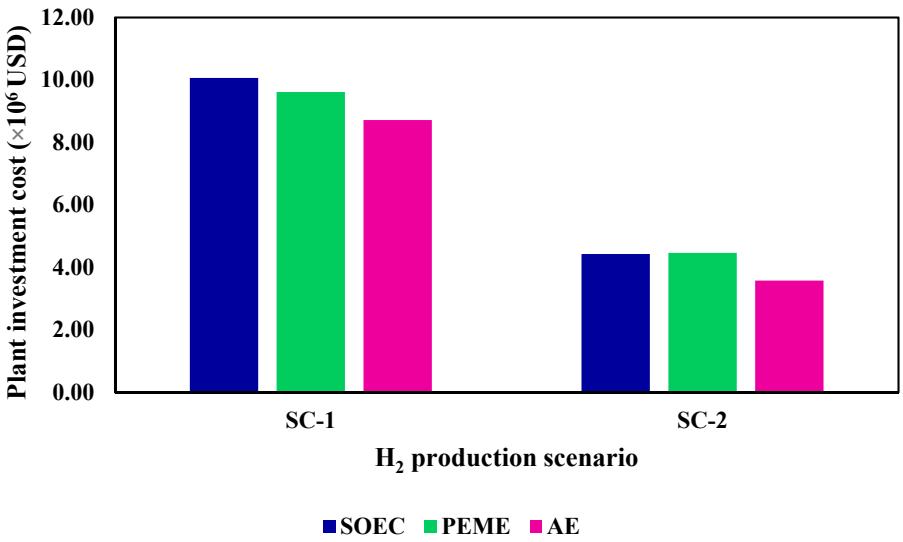

Figure 12. Investment cost of the H_2 production by the different electrolysis overall systems.

According to the results illustrated in Figure 13, the H_2 production cost including an AE electrolysis system is higher than PEME and SOEC, in this order, in both scenarios. In addition, in the case of SC-1, the H_2 production cost by the SOEC system is cheaper than AE and PEME systems by more than 6 USD/kg_{H2} and 4 USD/kg_{H2}, respectively. In the case of SC-2, there is a small difference between the LCOH registered by AE and PEME systems (0.24 USD/kg_{H2}), while SOEC is cheaper by more than 2 USD/kg_{H2} compared to both systems. This is due to the higher H_2 production by SOEC.

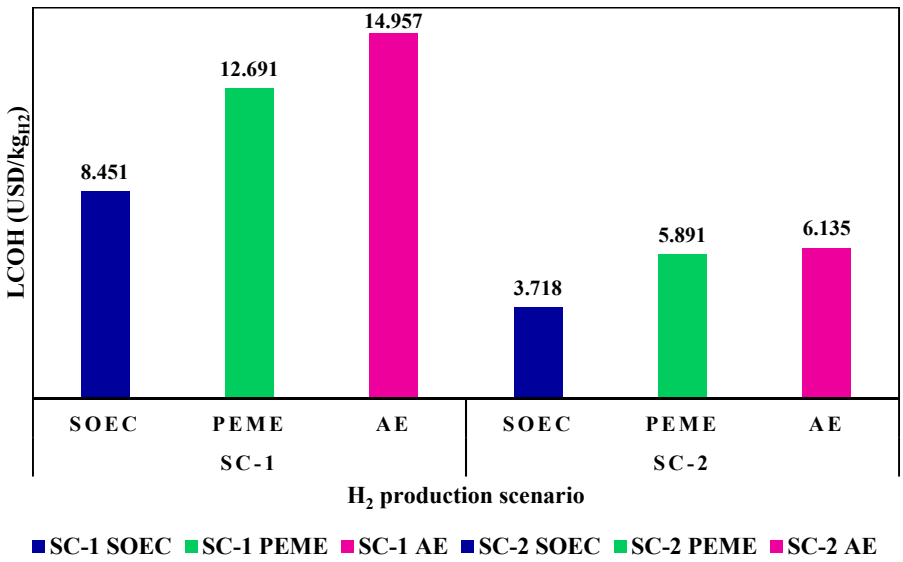

Figure 13. H_2 cost comparison.

7. Conclusions

The article investigates the H_2 production on board LNG carriers through three different electrolysis processes: AE, PEME, and SOEC. A comparison between the three electrolysers helps in ascertaining the most suitable and efficient technology for the onboard H_2 production. The required energy by the electrolysis stacks to drive the water splitting reactions is secured by the total WH energy of the LNG carrier's propulsion system through an ORC.

The electrolysis stacks are modelled through ACM V12.1 then exported to Aspen Hysys V12.1 for simulation with the rest of the plant component system. Aspen EDR V12.1

is used for the heat exchangers' design, while APEA is used for the economic analysis. According to the results, the main conclusions are as follows:

- SOEC consumes less energy (743.53 kW) than PEME (796.25 kW) and AE (797.69 kW), respectively, while producing more H_2, 21.94 kg/h compared to 13.96 kg/h by the PEME and 10.74 kg/h by the AE;
- The SOEC system electrolyser's efficiency (64.34%$_{LHV}$), ORC efficiency (12.8%), and overall system efficiency (10.59%) are all higher than those of PEME registering 58.33% for the electrolyser, 12.62% for the ORC, and 6.76% for the overall system; while AE registers 44.95% for the electrolyser, 12.62% for the ORC same as the PEME, and 5.2% for the overall system;
- Although the total investment cost of the plant including the SOEC system is higher than both PEME and AE, the LCOH of the overall SOEC system is lower by almost double in cost compared to PEME and AE.

To conclude, H_2 fuel is a promising alternative to fossil fuels in reducing emissions and aiming towards the decarbonisation of maritime transport. Among the three studied electrolysis systems, SOEC proves to be more advantageous than both PEME and AE for the onboard H_2 production as it consumes less energy while producing almost double the mass flow of H_2 per hr at a lower cost and being more efficient.

Supplementary Materials: The following supporting information can be downloaded at: https://www.mdpi.com/article/10.3390/jmse12081287/s1, Thermodynamic properties of the different studied systems.

Author Contributions: Conceptualisation, D.E., M.N., and M.R.G.; methodology, D.E., M.N., and M.R.G.; software, D.E., M.N., and M.R.G.; validation, M.N. and M.R.G.; formal analysis, D.E.; investigation, D.E.; writing—original draft preparation, D.E.; writing—review and editing, M.N. and M.R.G.; visualisation, D.E.; supervision, M.N. and M.R.G.; formal analysis, D.E. All authors have read and agreed to the published version of the manuscript.

Funding: Research contract funded by the Ferrol Industrial Campus under the Call "Talent in Training 2023" through the Research Center for Naval and Industrial Technologies (CITENI). Convenio Xunta de Galicia-Universidad de A Coruña: 2022/CP/139, Spain.

Institutional Review Board Statement: Not applicable.

Informed Consent Statement: Not applicable.

Data Availability Statement: The original contributions presented in the study are included in the article/Supplementary Material, further inquiries can be directed to the corresponding author.

Conflicts of Interest: The authors declare no conflicts of interest.

Nomenclature

A_{cl}	Cell area	$\dot{m}_{LNG}$	LNG mass flow rate
ACM	Aspen custom modeler	MSHEX	Multi-streams heat exchanger
AE	Alkaline electrolysis	N	Plant lifetime
an	Anode	N_{cl}	Number of stack cells
APEA	Aspen process economic analyser	NG	Natural gas
B_g	Flow permeability	NO_X	Nitrogen oxides
BOG	Boil-off gas	O_2	Oxygen
BOR	Design natural boil-off	O_{2perm}	O_2 permeation coefficient
C	Compressor	OP	Ozone depletion potential
Cat	Cathode	ORC	Conventional organic Rankine cycle

CEPCI	Chemical plant cost index
CO_2	Carbon dioxide
COND	Condenser
CRF	Capital recovery factor
d_a	Anode thickness
d_c	Cathode thickness
DF	Dual fuel
$D_{H2\text{-}H2O}$	Molecular diffusion
$D_{H2O\text{-}K}$	Knudsen diffusion
$E_{act,i}$	Activation energy at electrode i
ECO	Economiser
EDR	Aspen exchanger design and rating
E_{el}	Rate of the electric exergy input
EES	Engineering Equation Solver
EG	Exhaust gas
E_{H2}	Standard chemical exergy
E_{heat}	Rate of the thermal exergy input
ESS	Energy storage system
F	Faraday constant
Fr.W	Freshwater
FWG	Freshwater generator
GCU	Gas combustion unit
GEN	Generator
gH_2	Green hydrogen
GWP	Global warming potential
H_2	Hydrogen
H_{2perm}	H_2 permeation coefficient
HE	Heat exchanger
HFO	Heavy fuel oil
HHV	Higher heating value of H_2
HTO	Hydrogen to oxygen diffusion
i	Interest rate
ICE	Internal combustion engine
IMO	International maritime organisation
I_{st}	Stack current
J	Current density
$J_{0,i}$	Exchange current density at electrode i
$J_{exp,i}$	Pre-exponential factor at electrode i
JW	Jacket water
KOH	Potassium hydroxide
L	Electrolyte layer thickness
LCOH	Levelised cost of hydrogen
LHV	Lower heating value o H_2
LNG	Liquefied natural gas
$\dot{m}_{BOG}$	BOG mass flow rate
$\dot{m}_{BOGN}$	BOGN mass flow rate
MCR	Maximum continuous rating power
MDO	Marine diesel oil
M_j	Molecular mass of species j
OTH	Oxygen to hydrogen diffusion
P	Pressure
PEME	Proton exchange membrane electrolysis
P_j	Partial pressure of species j
Q_{av}	Available heat
Q_{excess}	Heat excess
$Q_{in\text{-}heat}$	Heat input
Q_{losses}	Heat losses
Q_{rec}	Recovered heat
Q_{st}	Electrolyser's heat
R	Gas constant
rad	Average pore radius
R_{el}	Overall ohmic resistance
S	Separator
SA	Scavenge air
SMR	Steam methane reforming
SOEC	Solid oxide electrolysis cell
T	Temperature
T_0	Reference environment temperature
$T_{W.hr}$	Working hours
V_0	Standard potential
V_{act}	Activation overpotential
V_{cl}	Cell voltage
V_{conc}	Concentration overpotential
V_{ohm}	Ohmic overpotential
V_{rev}	Reversible overpotential
V_{st}	Stack voltage
V_{tank}	Total cargo capacity
V_{th}	Thermoneutral voltage
W_{el}	Electrical energy
WH	Waste heat
WHR	Waste heat recovery
Z_{AE}	AE cost function
$Z_{O\&M}$	Operating and maintenance cost
Z_{PEME}	PEME cost function
ZSOEC	SOEC cost function
Ztotal	Total investment cost
ε	Electrode porosity
ε_{H2}/k	Lennard-Jones potential of hydrogen
ε_{H2O}/k	Lennard-Jones potential of steam
η	Efficiency
λi	Water content at anode and cathode
μ	Dynamic viscosity
ξ	Electrode tortuosity
ρ_{BOG}	BOG density
ρ_{LNG}	LNG density
σ_{H2}	Collision diameter of hydrogen
σ_{H2O}	Collision diameter of steam
Ω_D	Dimensionless diffusion

References

1. Kim, K.; Park, K.; Roh, G.; Chun, K. Case Study on Boil-Off Gas (BOG) Minimization for LNG Bunkering Vessel Using Energy Storage System (ESS). *J. Mar. Sci. Eng.* **2019**, *7*, 130. [CrossRef]
2. Livaniou, S.; Papadopoulos, G.A. Liquefied Natural Gas (LNG) as a Transitional Choice Replacing Marine Conventional Fuels (Heavy Fuel Oil/Marine Diesel Oil), towards the Era of Decarbonisation. *Sustainability* **2022**, *14*, 16364. [CrossRef]

3. Fernández, I.A.; Gomez, M.R.; Gómez, J.R.; López-González, L.M. Generation of H_2 on board LNG vessels for consumption in the propulsion system. *Pol. Marit. Res.* **2020**, *27*, 83–95. [CrossRef]
4. Aguilera, R.F.; Aguilera, R. World natural gas endowment as a bridge towards zero carbon emissions. *Technol. Forecast. Soc. Chang.* **2012**, *79*, 579–586. [CrossRef]
5. Fernández, I.A.; Gómez, M.R.; Gómez, J.R.; López-González, L.M. H_2 production by the steam reforming of excess boil off gas on LNG vessels. *Energy Convers. Manag.* **2017**, *134*, 301–313. [CrossRef]
6. Maxwell, D.; Zhu, Z. Natural gas prices, LNG transport costs, and the dynamics of LNG imports. *Energy Econ.* **2011**, *33*, 217–226. [CrossRef]
7. Kumar, S.; Kwon, H.-T.; Choi, K.-H.; Cho, J.H.; Lim, W.; Moon, I. Current status and future projections of LNG demand and supplies: A global prospective. *Energy Policy* **2011**, *39*, 4097–4104. [CrossRef]
8. Fernández, I.A.; Gómez, M.R.; Gómez, J.R.; Insua, Á.B. Review of propulsion systems on LNG carriers. *Renew. Sustain. Energy Rev.* **2017**, *67*, 1395–1411. [CrossRef]
9. Gómez, J.R.; Gómez, M.R.; Garcia, R.F.; Catoira, A.D.M. On board LNG reliquefaction technology: A comparative study. *Pol. Marit. Res.* **2014**, *21*, 77–88. [CrossRef]
10. Tu, H.; Fan, H.; Lei, W.; Zhou, G. Options and Evaluations on Propulsion Systems of LNG Carriers. In *Propulsion Systems*; Alessandro, S., Mario, P., Eds.; IntechOpen: Rijeka, Croatia, 2019; p. Ch. 1. [CrossRef]
11. Burel, F.; Taccani, R.; Zuliani, N. Improving sustainability of maritime transport through utilization of Liquefied Natural Gas (LNG) for propulsion. *Energy* **2013**, *57*, 412–420. [CrossRef]
12. Yeo, D.; Ahn, B.; Kim, J.; Kim, I. Propulsion alternatives for modern LNG carriers. In Proceedings of the Gas Technology Institute-15th International Conference and Exhibition on Liquefied Natural Gas, Barcelona, Spain, 24–27 April 2007.
13. Chang, D.; Rhee, T.; Nam, K.; Lee, S.; Kwak, B.; Ha, J. Economic evaluation of propulsion systems for LNG carriers: A comparative life cycle cost approach. *Hydrocarb. Asia* **2008**, *18*, 22–24,26,28.
14. Gómez, J.R.; Gómez, M.R.; Bernal, J.L.; Insua, A.B. Analysis and efficiency enhancement of a boil-off gas reliquefaction system with cascade cycle on board LNG carriers. *Energy Convers. Manag.* **2015**, *94*, 261–274. [CrossRef]
15. Dincer, I. Green methods for hydrogen production. *Int. J. Hydrogen Energy* **2012**, *37*, 1954–1971. [CrossRef]
16. Belz, S. A synergetic use of hydrogen and fuel cells in human spaceflight power systems. *Acta Astronaut.* **2016**, *121*, 323–331. [CrossRef]
17. Sebbahi, S.; Nabil, N.; Alaoui-Belghiti, A.; Laasri, S.; Rachidi, S.; Hajjaji, A. Assessment of the three most developed water electrolysis technologies: Alkaline Water Electrolysis, Proton Exchange Membrane and Solid-Oxide Electrolysis. *Mater. Today Proc.* **2022**, *66*, 140–145. [CrossRef]
18. Nejadian, M.M.; Ahmadi, P.; Houshfar, E. Comparative optimization study of three novel integrated hydrogen production systems with SOEC, PEM, and alkaline electrolyzer. *Fuel* **2023**, *336*, 126835. [CrossRef]
19. Zaccara, A.; Petrucciani, A.; Matino, I.; Branca, T.A.; Dettori, S.; Iannino, V.; Colla, V.; Bampaou, M.; Panopoulos, K. Renewable Hydrogen Production Processes for the Off-Gas Valorization in Integrated Steelworks through Hydrogen Intensified Methane and Methanol Syntheses. *Metals* **2020**, *10*, 1535. [CrossRef]
20. Nasser, M.; Hassan, H. Assessment of hydrogen production from waste heat using hybrid systems of Rankine cycle with proton exchange membrane/solid oxide electrolyzer. *Int. J. Hydrogen Energy* **2023**, *48*, 7135–7153. [CrossRef]
21. Ferrero, D.; Lanzini, A.; Santarelli, M.; Leone, P. A comparative assessment on hydrogen production from low- and high-temperature electrolysis. *Int. J. Hydrogen Energy* **2013**, *38*, 3523–3536. [CrossRef]
22. Dere, C.; Inal, O.B.; Zincir, B. Utilization of waste heat for onboard hydrogen production in ships. *Int. J. Hydrogen Energy* **2024**, *75*, 271–283. [CrossRef]
23. Wang, F.; Wang, L.; Zhang, H.; Xia, L.; Miao, H.; Yuan, J. Design and optimization of hydrogen production by solid oxide electrolyzer with marine engine waste heat recovery and ORC cycle. *Energy Convers. Manag.* **2021**, *229*, 113775. [CrossRef]
24. Delgado, M.S. Desarrollo y Validación de un Modelo para la Simulación de Sistemas de Electrólisis Alcalina para la Producción de Hidrógeno a Partir de Energías Renovables. Ph.D. Thesis, E.T.S.I. de Minas y Energía (UPM), Madrid, Spain, 2019.
25. Kumar, S.S.; Lim, H. An overview of water electrolysis technologies for green hydrogen production. *Energy Rep.* **2022**, *8*, 13793–13813. [CrossRef]
26. Burton, N.A.; Padilla, R.V.; Rose, A.; Habibullah, H. Increasing the efficiency of hydrogen production from solar powered water electrolysis. *Renew. Sustain. Energy Rev.* **2021**, *135*, 110255. [CrossRef]
27. Al-Douri, A.; Groth, K.M. Hydrogen production via electrolysis: State-of-the-art and research needs in risk and reliability analysis. *Int. J. Hydrogen Energy* **2024**, *63*, 775–785. [CrossRef]
28. Zhang, S.; Zhang, N. Review on integrated green hydrogen polygeneration system——Electrolysers, modelling, 4 E analysis and optimization. *J. Clean. Prod.* **2023**, *414*, 137631. [CrossRef]
29. IRENA. *Green Hydrogen Cost Reduction: Scaling Up Electrolysers to Meet the 1.5 °C Climate Goal*; International Renewable Energy Agency: Abu Dhabi, United Arab Emirates, 2020. Available online: https://www.irena.org/-/media/Files/IRENA/Agency/Publication/2020/Dec/IRENA_Green_hydrogen_cost_2020.pdf#page=12.00 (accessed on 4 April 2024).
30. Schmidt, O.; Gambhir, A.; Staffell, I.; Hawkes, A.; Nelson, J.; Few, S. Future cost and performance of water electrolysis: An expert elicitation study. *Int. J. Hydrogen Energy* **2017**, *42*, 30470–30492. [CrossRef]

31. Li, Y.; Lin, R.; O'Shea, R.; Thaore, V.; Wall, D.; Murphy, J.D. A perspective on three sustainable hydrogen production technologies with a focus on technology readiness level, cost of production and life cycle environmental impacts. *Heliyon* **2024**, *10*, e26637. [CrossRef] [PubMed]
32. Vidas, L.; Castro, R. Recent Developments on Hydrogen Production Technologies: State-of-the-Art Review with a Focus on Green-Electrolysis. *Appl. Sci.* **2021**, *11*, 11363. [CrossRef]
33. Buttler, A.; Spliethoff, H. Current status of water electrolysis for energy storage, grid balancing and sector coupling via power-to-gas and power-to-liquids: A review. *Renew. Sustain. Energy Rev.* **2018**, *82*, 2440–2454. [CrossRef]
34. Blender, A. LNG Ship. Sketchfab, Ed. Available online: https://sketchfab.com/3d-models/lng-ship-fa335b96450d4344863bbf5d912a0288 (accessed on 19 March 2024).
35. MAN. CEAS Engine Calculations. Available online: https://www.man-es.com/marine/products/planning-tools-and-downloads/ceas-engine-calculations (accessed on 19 March 2024).
36. HYUNDAI. Project Guide HIMSEN H35DF for Marine. 2022. Available online: https://www.hyundai-engine.com/en/Customer/TechData?page=4&category=all (accessed on 19 March 2024).
37. MAN. MAN B&W G70ME-C10.5-GI. Project Guide Electronically Controlled Dual Fuel Two-Stroke Engines. 2023. Available online: https://man-es.com/applications/projectguides/2stroke/content/printed/G70ME-C10_5-GI.pdf (accessed on 21 March 2024).
38. GTT. Available online: https://gtt.fr/technologies/markiii-systems (accessed on 19 March 2024).
39. Sprouse, C.; Depcik, C. Review of organic Rankine cycles for internal combustion engine exhaust waste heat recovery. *Appl. Therm. Eng.* **2013**, *51*, 711–722. [CrossRef]
40. Konur, O.; Yuksel, O.; Korkmaz, S.A.; Colpan, C.O.; Saatcioglu, O.Y.; Muslu, I. Thermal design and analysis of an organic rankine cycle system utilizing the main engine and cargo oil pump turbine based waste heats in a large tanker ship. *J. Clean. Prod.* **2022**, *368*, 133230. [CrossRef]
41. Singh, D.V.; Pedersen, E. A review of waste heat recovery technologies for maritime applications. *Energy Convers. Manag.* **2016**, *111*, 315–328. [CrossRef]
42. Mondejar, M.E.; Andreasen, J.G.; Pierobon, L.; Larsen, U.; Thern, M.; Haglind, F. A review of the use of organic Rankine cycle power systems for maritime applications. *Renew. Sustain. Energy Rev.* **2018**, *91*, 126–151. [CrossRef]
43. Baldasso, E.; Gilormini, T.J.A.; Mondejar, M.E.; Andreasen, J.G.; Larsen, L.K.; Fan, J.; Haglind, F. Organic Rankine cycle-based waste heat recovery system combined with thermal energy storage for emission-free power generation on ships during harbor stays. *J. Clean. Prod.* **2020**, *271*, 122394. [CrossRef]
44. Konur, O.; Colpan, C.O.; Saatcioglu, O.Y. A comprehensive review on organic Rankine cycle systems used as waste heat recovery technologies for marine applications. *Energy Sources Part A Recovery Util. Environ. Eff.* **2022**, *44*, 4083–4122. [CrossRef]
45. Zhu, S.; Zhang, K.; Deng, K. A review of waste heat recovery from the marine engine with highly efficient bottoming power cycles. *Renew. Sustain. Energy Rev.* **2020**, *120*, 109611. [CrossRef]
46. Andreasen, J.G.; Meroni, A.; Haglind, F. A Comparison of Organic and Steam Rankine Cycle Power Systems for Waste Heat Recovery on Large Ships. *Energies* **2017**, *10*, 547. [CrossRef]
47. Qyyum, M.A.; Khan, A.; Ali, S.; Khurram, M.S.; Mao, N.; Naquash, A.; Noon, A.A.; He, T.; Lee, M. Assessment of working fluids, thermal resources and cooling utilities for Organic Rankine Cycles: State-of-the-art comparison, challenges, commercial status, and future prospects. *Energy Convers. Manag.* **2022**, *252*, 115055. [CrossRef]
48. Díaz-Secades, L.A.; González, R.; Rivera, N.; Quevedo, J.R.; Montañés, E. Parametric study of organic Rankine working fluids via Bayesian optimization of a preference learning ranking for a waste heat recovery system applied to a case study marine engine. *Ocean Eng.* **2024**, *306*, 118124. [CrossRef]
49. Cataldo, F.; Mastrullo, R.; Mauro, A.W.; Vanoli, G.P. Fluid selection of Organic Rankine Cycle for low-temperature waste heat recovery based on thermal optimization. *Energy* **2014**, *72*, 159–167. [CrossRef]
50. Ata, S.; Kahraman, A.; Şahin, R.; Aksoy, M. Thermo-enviro-economic analysis of different power cycle configurations for green hydrogen production from waste heat. *Energy Convers. Manag.* **2024**, *301*, 118072. [CrossRef]
51. Larsen, U.; Pierobon, L.; Haglind, F.; Gabrielii, C. Design and optimisation of organic Rankine cycles for waste heat recovery in marine applications using the principles of natural selection. *Energy* **2013**, *55*, 803–812. [CrossRef]
52. ASHRAE. Designation and Safety Classification of Refrigerants. 2019. Available online: https://www.ashrae.org/file%20library/technical%20resources/standards%20and%20guidelines/standards%20addenda/34_2019_f_20191213.pdf (accessed on 19 July 2024).
53. Kumar, S.S.; Himabindu, V. Hydrogen production by PEM water electrolysis—A review. *Mater. Sci. Energy Technol.* **2019**, *2*, 442–454. [CrossRef]
54. Abdin, Z.; Zafaranloo, A.; Rafiee, A.; Mérida, W.; Lipiński, W.; Khalilpour, K.R. Hydrogen as an energy vector. *Renew. Sustain. Energy Rev.* **2020**, *120*, 109620. [CrossRef]
55. Wang, Z.; Wang, Y.; Afshan, S.; Hjalmarsson, J. A review of metallic tanks for H2 storage with a view to application in future green shipping. *Int. J. Hydrogen Energy* **2021**, *46*, 6151–6179. [CrossRef]
56. Wang, F.; Wang, L.; Ou, Y.; Lei, X.; Yuan, J.; Liu, X.; Zhu, Y. Thermodynamic analysis of solid oxide electrolyzer integration with engine waste heat recovery for hydrogen production. *Case Stud. Therm. Eng.* **2021**, *27*, 101240. [CrossRef]

57. Sánchez, M.; Amores, E.; Abad, D.; Rodríguez, L.; Clemente-Jul, C. Aspen Plus model of an alkaline electrolysis system for hydrogen production. *Int. J. Hydrogen Energy* **2020**, *45*, 3916–3929. [CrossRef]
58. Bianchi, F.R.; Bosio, B. Operating Principles, Performance and Technology Readiness Level of Reversible Solid Oxide Cells. *In Sustainability* **2021**, *13*, 4777. [CrossRef]
59. Sánchez, M.; Amores, E.; Rodríguez, L.; Clemente-Jul, C. Semi-empirical model and experimental validation for the performance evaluation of a 15 kW alkaline water electrolyzer. *Int. J. Hydrogen Energy* **2018**, *43*, 20332–20345. [CrossRef]
60. AspenTech. *Integrated Custom Model of Alkaline Electrolysis System for H2 Production*; AspenTech: Bedford, MA, USA, 2021.
61. Ulleberg, Ø. Modeling of advanced alkaline electrolyzers: A system simulation approach. *Int. J. Hydrogen Energy* **2003**, *28*, 21–33. [CrossRef]
62. Dincer, I.; Rosen, M.A.; Ahmadi, P. *Optimization of Energy Systems*; John Wiley & Sons Ltd: Chichester, UK, 2017; p. 472. [CrossRef]
63. Nami, H.; Akrami, E. Analysis of a gas turbine based hybrid system by utilizing energy, exergy and exergoeconomic methodologies for steam, power and hydrogen production. *Energy Convers. Manag.* **2017**, *143*, 326–337. [CrossRef]
64. Ni, M.; Leung, M.K.H.; Leung, D.Y.C. Energy and exergy analysis of hydrogen production by a proton exchange membrane (PEM) electrolyzer plant. *Energy Convers. Manag.* **2008**, *49*, 2748–2756. [CrossRef]
65. Mohtaram, S.; Wu, W.; Aryanfar, Y.; Yang, Q.; Alcaraz, J.L.G. Introducing and assessment of a new wind and solar-based diversified energy production system intergrading single-effect absorption refrigeration, ORC, and SRC cycles. *Renew. Energy* **2022**, *199*, 179–191. [CrossRef]
66. Mohammadi, A.; Mehrpooya, M. Techno-economic analysis of hydrogen production by solid oxide electrolyzer coupled with dish collector. *Energy Convers. Manag.* **2018**, *173*, 167–178. [CrossRef]
67. Ni, M.; Leung, M.K.H.; Leung, D.Y.C. Parametric study of solid oxide steam electrolyzer for hydrogen production. *Int. J. Hydrogen Energy* **2007**, *32*, 2305–2313. [CrossRef]
68. Visitdumrongkul, N.; Tippawan, P.; Authayanun, S.; Assabumrungrat, S.; Arpornwichanop, A. Enhanced performance of solid oxide electrolysis cells by integration with a partial oxidation reactor: Energy and exergy analyses. *Energy Convers. Manag.* **2016**, *129*, 189–199. [CrossRef]
69. Im-orb, K.; Visitdumrongkul, N.; Saebea, D.; Patcharavorachot, Y.; Arpornwichanop, A. Flowsheet-based model and exergy analysis of solid oxide electrolysis cells for clean hydrogen production. *J. Clean. Prod.* **2018**, *170*, 1–13. [CrossRef]
70. Zhao, Y.; Xue, H.; Jin, X.; Xiong, B.; Liu, R.; Peng, Y.; Jiang, L.; Tian, G. System level heat integration and efficiency analysis of hydrogen production process based on solid oxide electrolysis cells. *Int. J. Hydrogen Energy* **2021**, *46*, 38163–38174. [CrossRef]
71. AlZahrani, A.A. Investigation of a Novel High Temperature Solid Oxide Electrolyzer for Solar Hydrogen Production. Ph.D. Thesis, University of Ontario Institute of Technology, Oshawa, ON, Canada, 2017.
72. Luo, Y.; Wu, X.-y.; Shi, Y.; Ghoniem, A.F.; Cai, N. Exergy analysis of an integrated solid oxide electrolysis cell-methanation reactor for renewable energy storage. *Appl. Energy* **2018**, *215*, 371–383. [CrossRef]
73. Zhang, S.; Zhang, N.; Smith, R.; Wang, W. A zero carbon route to the supply of high-temperature heat through the integration of solid oxide electrolysis cells and H_2–O_2 combustion. *Renew. Sustain. Energy Rev.* **2022**, *167*, 112816. [CrossRef]
74. Christensen, A. Assessment of Hydrogen Production Costs from Electrolysis: United States and Europe. 2020. Available online: https://theicct.org/wp-content/uploads/2021/06/final_icct2020_assessment_of-_hydrogen_production_costs-v2.pdf (accessed on 7 March 2024).
75. Naeini, M.; Cotton, J.S.; Adams, T.A., II. An eco-technoeconomic analysis of hydrogen production using solid oxide electrolysis cells that accounts for long-term degradation. *Front. Energy Res.* **2022**, *10*, 1015465. [CrossRef]
76. Querol, E.; Gonzalez-Regueral, B.; Perez-Benedito, J.L. *Practical Approach to Exergy and Thermoeconomic Analyses of Industrial Processes*; Springer: London, UK, 2013.
77. The-University-of-Manchester-Department-of-Chemical-Engineering. Chemical Engineering Plant Cost Index. 2024. Available online: https://www.training.itservices.manchester.ac.uk/public/gced/CEPCI.html?reactors/CEPCI/index.html (accessed on 7 March 2024).